JPET Fast Forward. Published on October 10, 2012 as DOI: 10.1124/jpet.112.199497



**TITLE PAGE**

# Evaluation of Metabolically Stabilized Angiotensin IV Analogs as Pro-Cognitive/Anti-Dementia Agents

Alene T. McCoy, Caroline C. Benoist, John W Wright, Leen H. Kawas, Jyote M. Bule-Ghogare, Mingyan Zhu, Suzanne M. Appleyard, Gary A. Wayman and Joseph W. Harding

Department of Veterinary and Comparative Anatomy, Pharmacology, and Physiology, Washington State University, Pullman, WA- ATM, CCB, JWW, LHK, JB, MZ, SMA, GAW, JWH

Department of Psychology, Washington State University, Pullman, WA-JWW, JWH

Program in Pharmacology and Toxicology Washington State University, Pullman, WA- ATM, LHK, JWH

JPET Fast Forward. Published on October 10, 2012 as DOI: 10.1124/jpet.112.199497
This article has not been copyedited and formatted. The final version may differ from this version.



**RUNNING TITLE PAGE**

a) Running title page: Anti-dementia activity of stabilized angiotensin IV analogs

b) Corresponding author:

Dr. Joseph W Harding
Department of Veterinary and Comparative
Anatomy, Pharmacology, and Physiology
PO Box 6520
Washington State University
Pullman, WA 99164-6520 USA
Phone: 509 335-7927
FAX: 509 335-4652
E-mail: hardingj@vetmed.wsu.edu

c) Number of text pages:

Number of figures: 13 including 5 supplemental

Number of References: 41

Word count: Abstract- 207

Introduction- 486

Discussion- 756

List of non-standard abbreviations:

ACN: acetonitrile; Nle$^{1}$-AngIV: Nle-Tyr-Ile-His-Pro-Phe; Dihexa: N-hexanoic-Tyr-Ile-(6) amino-hexanoic amide; HGF: Hepatocyte Growth Factor; AUC: area under the concentration-time; $C_{max}$: concentration in plasma extrapolated to time zero ($C_0$); $t_{1/2:}$ terminal elimination rate constant; Vd: volume of distribution; CL: clearance; $Cl_{int}$: average intrinsic clearance; Cp0: plasma concentration at time zero; KE: elimination half-life; logP: log transformation of the octanol:water partition ratio and is a measure of hydrophilicity; $P_{eff}$ : predicted effective human

jejunal permeability; $P_{avg}$: predicted average intestinal permeability along the entire human intestinal tract ; $Pr_{Unbnd}$: percent of drug not bound to plasma proteins

d) Recommended section assignment: Drug discovery and translational medicine.

JPET Fast Forward. Published on October 10, 2012 as DOI: 10.1124/jpet.112.199497
This article has not been copyedited and formatted. The final version may differ from this version.



## ABSTRACT

Angiotensin IV (AngIV: VYIHPF) related peptides have long been recognized as pro-cognitive agents with potential as anti-dementia therapeutics. Their development as useful therapeutics, however, has been limited by physiochemical properties that make them susceptible to metabolic degradation and impermeable to gut and blood-brain barriers. A previous study had demonstrated that the core structural information required to impart the pro-cognitive activity of the AngIV analog, Norleucine$^{1}$-angiotensin IV (Nle$^{1}$-AngIV), resides in its three N-terminal amino acids, Nle-Tyr-Ile. The goal of this project was to chemically modify this tripeptide in such a way as to enhance its metabolic stability and barrier permeability to produce a drug candidate with potential clinical utility. Initial results demonstrated that several N- and C-terminal modifications lead to dramatically improved stability while maintaining the capability to reverse scopolamine-induced deficits in Morris water maze performance and augment hippocampal synaptogenesis. Subsequent chemical modifications, which were designed to increase hydrophobicity and decrease hydrogen bonding, yielded an orally active, blood-barrier permeant, metabolically stabilized analog, N-hexanoic-Tyr, Ile-(6) aminohexanoic amide (dihexa) that exhibits excellent anti-dementia activity in the scopolamine and aged rat models and marked synaptogenic activity. These data suggest that dihexa may have therapeutic potential as a treatment for disorders, like Alzheimer's disease, where augmented synaptic connectivity may be beneficial.

## INTRODUCTION

Multiple studies have documented the ability AngIV and several AngIV analogs to facilitate long-term potentiation, learning, and memory consolidation (Braszko et al., 1988; Wright et al., 1999; Kramar et al., 2001; Lee et al., 2004), increase cerebral blood flow (Kramar et al., 1997), and provide neuroprotection (Faure et al., 2006). More significantly the acute application of AngIV or one of its analogs, Nle$^1$-AngIV, reverses deficits in dementia models induced by: 1) treatment with the cholinergic muscarinic receptor antagonist scopolamine (Pederson et al., 2001); 2) kainic acid injections into the hippocampus (Stubley-Weatherly et al., 1996); 3) perforant path cuts (Wright et al., 1999); and 4) ischemia resulting from transient four vessel occlusion (Wright et al., 1996).

These observations have long encouraged the notion that AngIV-based pharmaceuticals may have potential as anti-dementia therapeutics (Mustafa et al., 2001; von Bohlen und Halbach, 2003; Gard, 2004, 2008; De Bundel et al., 2008; Wright and Harding, 2008). The transformation of AngIV and earlier described analogs into clinically useful agents has been impeded by their lack of metabolic stability and inability to penetrate the blood-brain barrier (BBB). This later limitation of AngIV–related peptides results from considerations of molecular size, overall hydrophobicity, and hydrogen bonding potential as reflected by the size of the encompassing hydration sphere. In an initial attempt to transform the highly active AngIV analog, Nle$^1$-AngIV, into an effective drug, we evaluated the pro-cognitive activity of a series of C-terminal truncated peptides derived from Nle$^1$-AngIV (Benoist et al., 2011). These initial studies

demonstrated that fragments as small at tri- and tetra-peptides retained the desired pro-cognitive/anti-dementia of Nle[1]-AngIV. Furthermore, the Benoist et al. study identified a likely explanation for the observed activity; namely, the capacity to augment synaptic connectivity through the induction of new functional synapses. Increased functional connectivity could be inferred from the augmented spinogenesis, the colocalizaion of synaptic markers on the newly formed dendritic spines and a concomitant enhancement of miniature excitatory postsynaptic currents.

The practical outcome of the Benoist et al. study was that the information required to support Nle[1]-AngIV-dependent pro-cognitive activity resided in the N-terminal tripeptide. This realization suggested that, with proper medicinal chemical modifications, it may be possible to develop clinically useful small molecule cognitive enhancers derived from Nle[1]-AngIV. Despite the small size of the tri- and tetra-peptides, a property ultimately necessary for BBB permeability, these molecules were metabolically unstable and likely too hydrophilic to breach the BBB. Thus, using these as templates we set out to increase metabolic stability and hydrophobicity by incorporating various structural changes that were primarily targeted at the N-terminal, the primary site of peptidase-dependent degradation (Abhold and Harding, 1988).

The results of the study described here indicated that N-terminal modifications, and to a lesser extent C-terminal modifications, could improve the metabolic stability of Nle[1]-AngIV-derived tri- and tetra-peptides while preserving pro-cognitive and synaptogenic activities. Expanding on these data additional modifications intended to increase hydrophobicity and decrease hydrogen bonding potential yielded N-hexanoic-

Tyr-Ile-(6)-aminohexanoic amide (dihexa), a potent cognitive enhancing molecule that proved to be very stable, capable of inducing spinogenesis/synaptogenesis at picomolar concentrations, slowly cleared from the blood compartment, and sufficiently BBB permeable.

JPET Fast Forward. Published on October 10, 2012 as DOI: 10.1124/jpet.112.199497
This article has not been copyedited and formatted. The final version may differ from this version.



## METHODS

### Compounds and peptide synthesis.

Scopolamine hydrobromide (#S-1875) was purchased from Sigma Chemical (St Louis, MO). The peptides were synthesized using Fmoc-based solid-phase peptide synthesis methods and purified by reverse phase HPLC in the Harding laboratory. Purity and structure were verified by LC-MS.

### Serum Metabolism of Peptides.

*Chemicals and reagents.* HPLC grade acetonitrile (ACN), acetic acid and water, and reagent grade trifluoroacetic acid (TFA) were purchased from Sigma/Aldrich (St Louis, MO). Norleucine-YIHPF ($Nle^1$-Ang-IV), D-Nle-YI, Acetyl-NleYIH, Gamma Amino Butyric Acid-YIH, NleYI-amide, N-hexanoic-YI-(6) aminohexanoic amide (dihexa) were synthesized by Fmoc based solid phase methods in the Harding laboratory.

*Animals and serum preparation.* Four month old male Sprague Dawley rats were used as the blood source for the metabolism studies. Blood was collected from left/right jugular veins of the rats using sterile catheters. After a 30 minute incubation on ice, the blood was centrifuged at 1000 rpm for 15 min to separate the serum. Serum was then transferred to clean tubes and stored at -20°C until use.

*Drug solution preparation.* Except for dihexa all drug solutions were prepared in HPLC grade water at 5 mg/ml. Stock drugs were kept in powder form and stored at -20ºC.

*Serum metabolism experimental procedure and analysis.* Rat blood serum samples were pre-equilibrated at 37ºC and then 10μL (50μg) of each drug solution was added to 90μL

of rat serum in 1.5mL Eppendorf tube maintained at 37ºC. At specified time intervals, metabolism was terminated by precipitating proteins with the addition of 1ml of a solution of acetonitrile (ACN) and acetic acid (9:1, v/v). The terminated reaction mixture was stored in refrigerator (5*ºC*) overnight and centrifuged (14,000 rpm) for 30 min to remove precipitated proteins. The separated supernatant was dried in Savant vacuum concentrator (Thermo Fisher, Asheville, NC). The dried samples were reconstituted using 200µL HPLC mobile phase (10% v/v ACN in water), vortexed briefly, and subjected to HPLC separation and analysis. A serum blank experiment to detect any interfering peaks in the HPLC chromatogram was performed by in an identical manner except that no drug was added. Zero time values for each drug candidate were established by first treating the serum with ACN, processing the sample as described above, adding drug, and then performing HPLC analysis.

The degradation rate of drug was determined by measuring the decrease in area under curve (AUC) at the retention time of drug over time. The AUC obtained from the zero time experiment was considered to represent the "100%" drug concentration and was used to determine the decreased drug concentration at each specified time interval. The semi-logarithmic plot of drug concentration vs. time was generated to determine degradation kinetic constant (k) of the tested drug. The half-life of drug was ($t_{1/2}$) was calculated by 0.693/k.

*Apparatus and chromatographic conditions.* Analysis of samples was performed using Shimadzu HPLC (Kyoto, Japan) system. The system consisted of a CBM-20A communications bus module, LC-20AB pumps, and a SPD-M20A photodiode array

detector. Data collection and integration were achieved using Shimadzu LC solution software. Separation was achieved using a Rainin Econosphere ODS C18 (250 mm x 4.6 mm id., 5 μm particle size) reverse phase column obtained from (Gilson, Middleton, WI). The column temperature was set at 40°C. The mobile phase consisted of a mixture of ACN and water with 0.1% TFA and was degassed by ultrasonication. Samples were introduced by manual mode with an injection volume of 250μL. The drug was eluted with a flow rate of 1mL/min and detected by PDA detector at excitation wavelengths of 215 and 280nm.

**IV Pharmacokinetics.**

*Animals and Surgical Procedures.* Male Sprague-Dawley rats (250+ g) were obtained from Harlan Laboratories (CA, USA) and allowed food (Harlan Teklad rodent diet) and water *ad libitum* in our animal facility. Ethics approval for animal experimentation was obtained from Washington State University. Rats were housed in temperature-controlled rooms with a 12 hour light/dark cycle. The right jugular veins of the rats were catheterized with sterile polyurethane Hydrocoat™ catheters (Access Technologies, Skokie, IL, USA) under ketamine (100 mg/kg im, Fort Dodge Animal Health, Fort Dodge, IA, USA) and isoflurane (Vet One™, MWI, Meridian, ID, USA) anesthesia. The catheters were exteriorized through the dorsal skin and flushed with heparinized saline before and after blood sample collection and filled with heparin-glycerol locking solution (6 mL glycerol, 3 mL saline, O.5 mL gentamycin (100mg/mL), 0.5 mL heparin (10,000 u/mL)) when not sampled for more than 8 hours.

*Blood Sample Preparation.* Fresh rat blood was obtained prior to each experiment via jugular vein catheters from adult male Sprague-Dawley rats.

Dihexa solutions were prepared by suspending dry stock dihexa in DMSO at 1mg/mL and subsequent serial dilutions in 50% DMSO or HPLC grade water for the final concentrations specified. Stock dihexa is kept in powder form and stored at -20ºC. Quality control (QC) samples were prepared by spiking fresh rat plasma with an appropriate dilution of dihexa for the final concentration of dihexa specified, keeping a 10:1 ratio of plasma to dihexa solution (final DMSO concentration 5%). The compounds, $Nle^1$-Ang-IV and Nle-YI-(6) aminohexanoic amide, molecules very similar in structure and properties to dihexa, were used as internal standards and were prepared the same way.

The proteins present in the plasma samples were precipitated using three volumes of ice-cold acetonitrile. Internal standards were then added and the samples were vortexed for approximately 10 seconds. Samples were then centrifuged at 5000 RPM for 5 minutes. The supernatants were transferred to new tubes and stored until use at -20ºC. Samples were then concentrated in a Savant SpeedVac® concentrator to a volume of approximately 100ul. 200ul HPLC grade water was added to each sample and the samples were transferred to autosampler vials.

*Pharmacokinetic Study*. Male Sprague Dawley rats were catheterized as described in the Animals and Surgical Procedures section. Animals were placed in metabolic cages prior to the start of the study and time zero blood and urine samples were collected. The animals were then dosed intravenously via the jugular vein catheters or intraperitoneally

with dihexa dissolved in 75% DMSO. The typical injection volume was 200µL yielding an initial estimated DMSO concentration in blood of 0.46%. After dosing, blood samples were collected as described in Table 1.

After each blood sample was taken, the catheter was flushed with heparinized lactated Ringer's solution and a volume of heparinized lactated Ringer's equal to the volume of blood taken was injected (to maintain total blood volume).

The blood samples were collected into polypropylene microcentrifuge tubes and cooled on ice for not more than 1 hour. The samples were centrifuged at 5000 RPM for 7 minutes and 80 µLplasma were transferred into previously prepared tubes containing 240 µL ice-cold acetonitrile. The samples were vortexed vigorously for 30 seconds and held on ice. 100 µg/mL Nle-YI-(6) aminohexanoic amide in 10 µL was used as an internal standard and added to each sample on ice. Samples were held on ice until the end of the experiment and stored at -20ºC afterward until further processing.

Serial dilutions of dihexa in 50% DMSO or water (for dilutions of 50 µg/mL or less) were prepared from the stock used to dose the animals to be used for preparation of a standard curve. 10 µL of each serial dilution was then added to 90 µL of blank plasma for final concentrations of 0.01, 0.02, 0.05, 0.1, 0.2, 1, 10, 20, 50 and 100 µg/mL. 80 µL of each plasma sample was transferred to previously prepared tubes containing 240 µL ice-cold acetonitrile and vortexed vigorously. 10 µL containing 100 µg/mL Nle-YI-(6) aminohexanoic amide as an internal standard, was added to each sample on ice. The standard curve plasma samples were then stored at -20ºC and further processed alongside the pharmacokinetic study samples according to the method described above.

*Chromatographic System and Conditions.* The HPLC/MS system that was employed was from Shimadzu (Kyoto, Japan), consisting of a CBM-20A communications bus module, LC-20AD pumps, SIL-20AC auto sampler, SPD-M20A diode array detector and LCMS-2010EV mass spectrometer. Data collection and integration were achieved using Shimadzu LCMS solution software.

The analytical column that was used was an Econosphere C18 (100mm x 2.1mm) from Grace Davison Discovery Science (Deerfield, IL, USA). The mobile phase consisted of HPLC grade acetonitrile and water with 0.1% acetic acid. For plasma samples, separation was carried out using a non-isocratic method, starting at 23% ACN and climbing to 31% ACN over 9 minutes, at ambient temperature and a flow rate of 0.3 mL/min. For MS analysis, a positive ion mode (SIM) was used to monitor the m/z of dihexa at 527 (dihexa with the addition of a sodium adduct) and the m/z of Nle-YI-(6) aminohexanoic amide and Nle$^{1}$- AngIV (internal standards) at 513 and 541, respectively (both with sodium adducts). Samples were introduced using the autosampler and the injection volume was 50ul. For the microsomal study, the m/z of verapamil was 455, the m/z of piroxicam was 332, and the m/z of 7-ethoxycoumarin was 191.

*Pharmacokinetic Analysis.* Pharmacokinetic analysis was performed using data from individual rats from which the mean and standard error of the mean (SEM) were calculated for each group. Noncompartmental pharmacokinetic parameters were calculated from plasma drug concentration-time profiles by use of WinNonlin® software (Pharsight, Mountain View, CA, USA). The following relevant parameters were determined where possible: area under the concentration-time curve from time zero to the

last time point ($AUC_{0\text{-}last}$) or extrapolated to infinity ($AUC_{0\text{-}\infty}$), $C_{max}$ concentration in plasma extrapolated to time zero ($C_0$), terminal elimination half-life ($t_{1/2}$), volume of distribution (Vd), and clearance (CL).

*Blood-Brain Barrier Penetrability Study*

To evaluate the of ability dihexa to penetrate the BBB and accumulate in the brain rats were fitted with carotid cannulas and infused with 10μCi of $^{3}$H-dihexa and 2μCi of $^{14}$C inulin, a vascular space marker, in 100μL of isotonic saline. Thirty minutes after infusion, brains were removed and dissected and blood samples taken. After solubilization, $^{3}$H and $^{14}$C were quantified by dual window scintillation counting to determine the amount of dihexa and inulin in brain and blood samples. The ratio of dihexa/inulin in blood was then used to account for any blood contamination in the various brain regions.

**Microsomal Metabolism.**

Male rat liver microsomes were obtained from Celsis (Baltimore, MD, USA). The protocol from Celsis for microsome-drug incubation was followed with minor adaptations. An NADPH regenerating system (NRS) was prepared as follows: 1.7 mg/mL NADP, 7.8 mg/mL glucose-6-phosphate and 6 units/mL glucose-6-phosphate dehydrogenase were added to 10 mL 2% sodium bicarbonate. The NRS was used immediately. 500 μM solutions of dihexa, piroxicam, verapamil and 7-ethoxycoumarin (low, moderate and highly metabolized controls, respectively) were prepared in acetonitrile. Microsomes were suspended in 0.1M Tris buffer (pH 7.38) at 0.5 mg/mL.

100 µL microsomes were added to pre-chilled microcentrifuge tubes on ice. To each sample, 640 µL 0.1M Tris buffer and 10 µL of 500 µM test compound were added. The samples and NRS were placed in a water bath at 37ºC for 5 minutes. Samples were removed from the water bath, 250 µL NRS was added, and each was placed into a rotisserie hybridization oven at 37ºC with rotation at high speed for the appropriate incubation time (10, 20, 30 40 or 60 minutes). 500 µL from each sample was transferred to each of two tubes containing 500 µL ice-cold acetonitrile with internal standard per incubation sample. Standard curve samples were prepared in incubation buffer and 500 µL was added to 500 µL of ice-cold acetonitrile with internal standard. All samples were then analyzed by high performance liquid chromatography/mass spectrometry. Drug concentrations were determined and loss of parent relative to negative control samples containing no microsomes was calculated. Clearance was determined by nonlinear regression analysis for $k_e$ and $t_{1/2}$ and the equation $Cl_{int} = k_e$ Vd.

**Behavioral Studies.**

*Animals and Surgery.* Male Sprague-Dawley rats (Taconic derived) weighing 390-450 g were maintained with free access to water and food (Harland Tekland F6 rodent diet, Madison, WI) except the night prior to surgery when food was removed were used for most studies. The aged rat study employed 24 month old rats of mixed sex. For the scopolamine studies each animal was anesthetized with Ketamine hydrochloride plus Xylazine (100 and 2 mg/kg im. respectively; Phoenix Scientific; St. Joseph, MO, and Moby; Shawnee, KS). When required an intracerebroventricular (icv) guide cannula (PE-60, Clay Adams; Parsippany, NY) was stereotaxically positioned (Model 900, David

Kopf Instruments; Tujunga, CA) in the right hemisphere using flat skull coordinates 1.0 mm posterior and 1.5 mm lateral to bregma (refer to Wright *et al.* 1985). The guide cannula measured 2.5 cm in overall length and was prepared with a heat bulge placed 2.5 mm from its beveled tip, thus acting as a stop to control the depth of penetration at 2.5mm. Once in position, the cannula was secured to the skull with two stainless-steel screws and dental cement. The guide was then sealed with a thick stainless steel wire. Post-operatively the animals were housed individually in an American Accreditation for Laboratory Animal Care-approved vivarium maintained at 22±1° C on a 12-h alternating light/dark cycle initiated at 06:00 h. All animals were hand gentled for 5 min per day during the 5-6 days of post-surgical recovery. Histological verification of cannula placement was accomplished by the injection of 5 µl fast-green dye via the guide cannula following the completion of behavioral testing. Correct cannula placement was evident in all rats utilized in this study.

*Water maze testing.* The water maze consisted of a circular tank painted black (diameter: 1.6 m; height: 0.6 m), filled to a depth of 26 cm with 26-28° C water. A black circular platform (diameter: 12 cm; height: 24 cm) was placed 30 cm from the wall and submerged 2 cm below the water surface. The maze was operationally sectioned into four equal quadrants designated NW, NE, SW, and SE. For each rat the location of the platform was randomly assigned to one of the quadrants and remained fixed throughout the duration of training. Entry points were at the quadrant corners (i.e. N, S, E, and W) and were pseudo-randomly assigned such that each trial began at a different entry point than the preceding trial. Three of the four testing room walls were covered with extra-maze spatial cues consisting of different shapes (circles, squares, triangles) and colors.

The swimming path of the animals was recorded using a computerized video tracking system (Chromotrack; San Diego Instruments, CA). The computer displayed total swim latency and swim distance. Swim speed was determined from these values.

Each member of the treatment groups received an icv injection of scopolamine hydrobromide (70 nmol in 2 µl aCSF over a duration of 20 s) 20 min prior to testing followed by $Nle^1$-AngIV or one of the analogs (in 2 µl aCSF) 5 min prior to testing. Control groups received scopolamine or aCSF 20 min prior to testing followed by aCSF 5 min prior testing. The behavioral testing protocol has been described previously in detail (Wright *et al.* 1999). Briefly, acquisition trials were conducted on 8 consecutive days with 5 trials/day. On the first day of training the animal was placed on the platform for 30 s prior to the first trial. Trials commenced with the placement of the rat facing the wall of the maze at one of the assigned entry points. The rat was allowed a maximum of 120 s to locate the platform. Once the animal located the platform it was permitted a 30 s rest period on the platform. If the rat did not find the platform, the experimenter placed the animal on the platform for the 30 s rest period. The next trial commenced immediately following the rest period.

On the day following acquisition training (day 9), one additional trial was conducted during which the platform was removed (probe trial). The animal was required to swim the entire 120 s to determine the persistence of the learned response. Total time spent within the target quadrant where the platform had been located during acquisition and the number of crossings of that quadrant was recorded. Upon completion of each daily set of

trials the animal was towel-dried and placed under a 100 watt lamp for 10-15 min and then returned to its home cage.

**Dendritic spine analysis.**

*Hippocampal cell culture preparation.* Hippocampal neurons ($2x10^5$ cells per square cm) were cultured from P1 Sprague Dawley rats on plates coated with poly-L-lysine from Sigma (St. Louis, MO; molecular weight -300,000). Hippocampal neurons were maintained in Neurobasal A media from Invitrogen (Carlsbad, CA) supplemented with B27 from Invitrogen, 0.5 mM L-glutamine, and 5mM cytosine-D-arabinofuranoside from Sigma added at 2 days *in vitro*. Hippocampal neurons were then cultured a further 3–7 days, at which time they were either transfected or treated with various pharmacological reagents as described in (Wayman et al., 2008).

*Transfection.* Neurons were transfected with mRFP-β-actin on day *in vitro* 6 (DIV6) using LipofectAMINE 2000 (Invitrogen) according to the manufacturer's protocol. This protocol yielded the desired 3-5% transfection efficiency thus enabling the visualization of individual neurons. Higher efficiencies obscured the dendritic arbor of individual neurons. Expression of fluorescently tagged actin allowed clear visualization of dendritic spines, as dendritic spines are enriched in actin. On DIV7 the cells were treated with vehicle ($H_20$) or peptides (as described in the text) added to media. On DIV12 the neurons were fixed (4% paraformaldehyde, 3% sucrose, 60 mM PIPES, 25 mM HEPES, 5 mM EGTA, 1 mM $MgCl_2$, pH 7.4) for 20 min at room temperature and mounted.

Slides were dried for at least 20 hours at 4°C and fluorescent images were obtained with Slidebook 4.2 Digital Microscopy Software driving an Olympus IX81 inverted confocal microscope with a 60X oil immersion lens, NA 1.4 and resolution 0.280 µm. Dendritic spine density was measured on primary and secondary dendrites at a distance of at least 150 µm from the soma. Five 50 µm long segments of dendrites from at least 10 neurons were analyzed for each data point reported. Each experiment was repeated at least three times using independent culture preparations. Dendrite length was determined using the National Institutes of Health's Image J 1.41o program (NIH, Bethesda, MD) and the neurite tracing program Neuron J (Meijering et al., 2004) Spines were manually counted.

*Organotypic hippocampal slice culture preparation and transfection.* Hippocampi from P4 Sprague Dawley rats were cultured as previously described (Wayman, Impey et al. 2006). In order to visualize dendritic arbors 400 µm hippocampal slices from postnatal day 5 were cultured for 3 days after which they were biolistically transfected with tomato fluorescent protein (TFP) using a Helios Gen Gun (BioRad, Hercules, CA), according to the manufacturer's protocol. Following a 24 hour recovery period slices were stimulated with vehicle ($H_2O$), 1pM $Nle^1$-AngIV or dihexa for 2 days. Slices were fixed and mounted. Hippocampal CA1 neuronal processes were imaged and measured as described above.

*Immunocytochemistry.* Transfected neurons were treated and fixed as described above. Following fixation, cells were rinsed in PBS and permeabilized with 0.1% Triton X-100 detergent (Bio-Rad; Hercules, CA), followed by two rinses in PBS and blocked with 8% bovine serum albumin (Intergen Company; Burlington, MA) in PBS for 1 h. Cells were

again rinsed with PBS, followed by a 24 hour incubation period with anti- α-VGLUT1 (Synaptic Systems; Goettingen, Germany) , anti-synapsin (Synaptic Systems; Goettingen, Germany), anti-PSD-95 (Milipore, Billerica, MA) following the manufacturers protocol, at 4°C. Subsequently cells were rinsed twice with PBS, incubated in Alexafluor 488 goat-anti-mouse following the manufacturer's protocol (Invitrogen: Carlsbad, CA) for two hours at room temperature, rinsed again with PBS, and mounted with ProLong Gold anti-fade reagent (Invitrogen; Carlsbad, CA). Imaging and analysis were performed as described above.

*Whole-cell recordings.* Patch-clamp experiments were performed on mRFP-β-actin transfected cultured hippocampal neurons with PBS (vehicle control) or 1pM $Nle^1$-AngIV pretreatment. Recordings were made on DIV12-14. The culture medium was exchanged by an extracellular solution containing (in mM) 140 NaCl, 2.5 KCl, 1 MgCl2, 3 CaCl2, 25 glucose, and 5 HEPES; pH was adjusted to 7.3 with KOH; and osmolality was adjusted to 310 mOsm. Cultures were allowed to equilibrate in a recording chamber mounted on inverted microscope (IX-71; Olympus optical, Tokyo) for 30 min. before recording. Transfected cells were visualized with fluorescence (Olympus optical). Recording pipettes were pulled (P-97 Flaming/Brown micropipette puller; Sutter Instrument, Novato, CA) from standard-wall borosilicate glass without filament (OD = 1.5 mm; Sutter Instrument). The pipette-to-bath DC resistance of patch electrodes ranged from 4.0 to 5.2MΩ, and were filled with an internal solution of the following composition (in mM): 25 CsCl, 100 CsCH3O3S, 10 phosphocreatine, 0.4 EGTA, 10 HEPES, 2 MgCl2, 0.4 Mg-ATP, and 0.04 Na-GTP; pH was adjusted to 7.2 with CsOH; osmolality was adjusted to 296 - 300 mOsm. Miniature EPSCs (mEPSCs) were isolated

pharmacologically by blocking GABA receptor chloride channels with picrotoxin (100 μM; Sigma), blocking glycine receptors with strychnine (1 μM; Sigma), and blocking action potential generation with tetrodotoxin (TTX, 500 nM; R&D Systems, Minneapolis, MN ). Recordings were obtained using a Multiclamp 700B amplifier (Molecular Devices, Sunnyvale, CA). Analog signals were low-pass Bessel filtered at 2 kHz, digitized at 10 kHz through a Digidata 1440A interface (Molecular Devices), and stored in a computer using Clampex 10.2 software (Molecular Devices). The membrane potential was held at -70 mV at room temperature (25ºC) during a period of 0.5-2 h after removal of the culture from the incubator. Liquid junction potentials were not corrected. Data analysis was performed using Clampfit 10.2 software (Molecular Devices), and Mini-Analysis 6.0 software (Synaptosoft Inc.; Fort Lee, NJ). The criteria for a successful recording included an electrical resistance of the seal between the outside surface of the recording pipette and the attached cell >2 GΩ and a neuron input resistance >240 MΩ. The mEPSCs had a 5-min recording time.

**Statistical Analyses.**

The Morris water maze data sets, consisting of mean latencies and path distances to find the platform during each daily block of five trials, were calculated for each animal for each day of acquisition. One-way ANOVAs were used to compare group swim latencies on Days 1, 4, and 8 of training. Past experience with this task has indicated these days to be representative of overall performance. Data collected during the probe trials (time spent in the target quadrant and entries into the target quadrant) were also analyzed using one-way ANOVAs. Significant effects were further analyzed by a

Newman-Keuls post-hoc test with a level of significance set at $p < 0.05$. Because of variability in the non-treated aged rat group a non-parametric Mann-Whitney U test was performed to evaluate significance.

One-way ANOVA was used to analyze the dendritic spine results and significant effects were analyzed by Tukey post-hoc test. Linear regression analysis was used to determine the correlation between spine characteristics and latency to find the platform in the water maze task. Multiple comparisons of electrophysiological results were made using a one-way ANOVA followed by a Newman-Keuls post-hoc test with a level of significance set at $p < 0.05$. Numerical data are expressed as mean ± SEM.

## RESULTS

### *N- and C- terminal modifications of Nle$^1$-AngIV-derived peptides exhibit improved stability in rat serum*

In our quest to develop a BBB permeable Nle$^1$-AngIV-derived molecule with pro-cognitive activity we have recently determined that the Nle$^1$-AngIV-derived N-terminal tri- and tetra-peptides possess full biological activity (Benoist et al., 2011). This observation was critical to reaching our ultimate goal because smaller molecules have a higher probability of breaching the BBB than larger ones. With this foundation the next task was to improve the metabolic stability of Nle$^1$-AngIV-derived N-terminal tri- and tetra-peptides. Previous studies by our laboratory have indicated that angiotensin-like peptides are rapidly metabolized in vivo through the action of aminopeptidases (Dewey et al., 1988). As such, we introduced several structural changes directed at the N-terminal including: the substitution of D-norleucine for L-norleucine; the N-acetylation of norleucine; and the replacement of norleucine with a non-α-amino acid γ-aminobutyric acid (GABA) with an expectation of reduced susceptibility to aminopeptidases and overall improved stability. In addition, the impact of converting the C-terminal carboxylic acid to an amide on metabolic stability was also examined.

To evaluate the effect of these structural changes on general metabolic stability the compounds were incubated in the presence of rat serum and the resultant incubates analyzed for metabolism by HPLC. The results of this study, which are shown in **Table 2,** indicate that as expected Nle$^1$-AngIV had an exceedingly short half-life of less than two minutes; while each of the N-terminal modified peptides exhibited markedly

elongated half-lives. A more modest increase in stability was noted following C-terminal amidation. These data confirm the importance of attenuating N-terminal dependent degradation, if one desires to improve the metabolic stability of Nle$^1$-AngIV-derived peptides. Thus, the incorporation of these types of modifications or the introduction of non-peptide bonds (Krebs et al., 1996) may provide a workable strategy to improve the bioavailability of Nle$^1$-AngIV-derived peptides and peptidomimetics.

***N- and C-terminal modified Nle$^1$-AngIV analogs retain pro-cognitive activity.***

While N-terminal modification of Nle$^1$-AngIV-derived tri- and tetra-peptides significantly increased their stability in rat serum the true test of success of these structural modifications is whether the molecules still possess pro-cognitive activity. To gauge the pro-cognitive potential of the molecules we evaluated their capacity to reverse scopolamine-dependent learning deficits following their acute ICV application as assessed by performance in the Morris water maze. The scopolamine preparation that was employed is a widely accepted animal model of the spatial memory dysfunction and produces deficits reminiscent of those observed in early to middle stage Alzheimer's disease patients (Fisher et al., 2003).

As an initial measure of cognitive function, the escape latency to locate the submerged pedestal in a Morris water maze was recorded over an eight day observation period. As can be seen in **Figure 1A**, scopolamine application significantly retarded task acquisition when compared to vehicle controls. Tandem application of scopolamine with each of the N-and C-terminal modified peptides significantly improved water maze performance when compared to the scopolamine treated group. Although there were no

differences among the groups on Day 1 of training, all the compound treated groups showed improved performance by Day 3 ( $p<0.001$). This improved performance was maintained throughout the testing period and post-hoc analyses on Day 8 confirmed that all had improved performance when compared to the scopolamine/deficit group ($p<0.0001$). On day 8 animals treated with the GABA-Tyr-Ile exhibited the best performance among the compound treated groups, had a significantly lower mean latency to find the platform than the other three treated groups ($p<.001$), which did not differ from one another ($p>.05$), and was not significantly different than the vehicle control group ($p>.05$).

As a second measure of cognitive function, the persistence and strength of the learned task was assessed with a probe trial on Day 9 (**Figure 1B**). The rats were exposed to the maze with no pedestal for two minutes and time spent in the quadrant that originally contained the submerged pedestal was determined. These data mirrored the escape latency results with all treated groups performing better than the scopolamine/deficit group ($p<.01$-$.001$). Again the performance by the group treated with GABA-Tyr performance was superior to all the other compound treated groups ($p<.05$-$.01$) and not different from the vehicle control group ($p>.05$).

***N- and C-terminal modified Nle$^1$-AngIV analogs stimulate dendritic spinogenesis.***

As part of our a recent evaluation of C-terminal truncated fragments of Nle$^1$-AngIV, we demonstrated that Nle$^1$-AngIV and only its cognitively active C-terminal truncated fragments were effective stimulators of dendritic spinogenesis on cultured hippocampal neurons from neonatal rats. As such, the expectation was that the

cognitively active fragments described here would also support hippocampal spinogenesis. As can be seen from the dose-response curves presented in **Supplemental Figure 1 (A-D)**, this expectation was borne out for each of the metabolically stabilized molecules. The only surprise from this study was that GABA-Tyr-Ile, which had consistently exhibited the most profound pro-cognitive activity, did not appear to be the most potent generator of new dendritic spines.

***N-hexanoic-Tyr-Ile-(6)aminohexanoic amide (dihexa) is a metabolically stabilized, blood-brain barrier permeable molecule.***

The data presented in **Table 1** indicate that increased stability can be imparted to $Nle^1$-AngIV-derived compounds by both N- and C-terminal modification. In addition, the functional studies summarized in **Figure 1** indicate that replacement of norleucine in the number one position with the straight chain, non-α-amino acid GABA yielded a molecule with superior pro-cognitive activity. With this information in hand we synthesized a series of compounds, exemplified by dihexa, that not only were protected at both terminals, but contained the replacement of norleucine with a straight chain acyl group. Instead of simply appending a non-α-amino long straight chain amino acid to the N-terminal we chose to eliminate the N-terminal amine entirely, which increased overall hydrophobicity and removed a critical hydrogen bonding site. As can be seen in **Table 2** these modification significantly increased the serum stability of dihexa in comparison to $Nle^1$-AngIV.

The purpose of elongating the N-terminal acyl group and removing the N-terminal amino group was to increase the probability that resultant molecules might be

BBB permeable and access the brain parenchyma. To evaluate the success of the modifications that were incorporated in dihexa in this regard rats were fitted with carotid cannulas and infused with 10μCi of $^{3}$H-dihexa and 2μCi of $^{14}$C inulin, a vascular space marker. Thirty minutes after infusion, brains were removed and dissected and blood samples taken. After solubilization, $^{3}$H and $^{14}$C were quantified by dual window scintillation counting to determine the amount of dihexa and inulin in brain and blood samples. The ratio of dihexa/inulin in blood was then used to account for any blood contamination in the various brain regions. More importantly, $^{3}$H/$^{14}$C ratios above that observed in blood were indicative of dihexa being concentrated. As can be seen in **Figure 2,** all the brain regions examined avidly concentrated dihexa attesting to its ability to cross the BBB.

***Dihexa has a long circulating half-life.***

To begin to evaluate the potential clinical utility of dihexa Adult male Sprague-Dawley rats were administered 10 mg/kg dihexa intravenously and *in-vivo* pharmacokinetics determined. An example of the resulting plasma concentration/time profile is shown in **Supplemental Figure 2**. dihexa exhibited rapidly decreasing plasma levels from 0 to 4 hours suggesting that both distribution and elimination occurred during this period. After 4 hours, the rate of clearance declined and plasma levels became more stable, exhibiting a relatively linear rate of decline suggesting a phase of pure elimination from 4 to 120 hours. The exception from the linearly declining pattern of plasma levels was between 8.5 to 13 hours, when plasma levels were actually lower than at 24 hours. These results suggest that a small fraction of dihexa undergoes enterohepatic recirculation, which could cause an increase in plasma levels. Elevations in plasma

concentration due to enterohepatic recirculation are usually observed after a meal when bile containing drug is released into the duodenum and the drug is reabsorbed from the intestine (Kwon 2001). Since rats were allowed food 12 hours after the onset of the study, any enterohepatic recirculation would be expected to occur subsequent to 12 hours, the time period that corresponded with rising plasma levels of dihexa.

Relevant pharmacokinetic parameters for dihexa as determined after IV dosing are summarized in **Table 3**. Plasma data were modeled by non-compartmental analysis using WinNonlin® software. dihexa exhibited a long half-life ($t_{1/2}$) of 12.68 days following IV administration and similarly when delivered intraperitoneally (8.83+/- 2.41 days, Mean +/-SEM; N=4). dihexa appeared to be extensively distributed outside the central blood compartment and/or bound within the tissues as evidenced by its large volume of distribution (Vd). These results, which suggest that dihexa is very hydrophobic (logP) and are in agreement with the outcome of QSAR modeling estimates generated by ADMET Predictor® that calculated an octanol:water partition coefficient of 177.8 for dihexa (**Table 4**).

Not surprisingly because of its stability, hydrophobic character, and small size, dihexa was predicted to be orally bioavailable. The $P_{eff}$ value represents the predicted effective human jejunal permeability of the molecule (**Table 4**). The predicted $P_{eff}$ value for dihexa (1.78) is intermediate between the predicted $P_{eff}$ values for enalapril (1.25) and piroxicam (2.14), two orally bioavailable drugs. dihexa was also predicted to be 22.59 percent unbound to plasma proteins in circulation, thus making it available for distribution into the tissues.

JPET Fast Forward. Published on October 10, 2012 as DOI: 10.1124/jpet.112.199497
This article has not been copyedited and formatted. The final version may differ from this version.



Also contributing to its slow removal from the blood was a lack of Phase I metabolism for dihexa. Phase I metabolism of dihexa, which was determined using pooled male rat liver microsomes, was found to be very low with an average intrinsic clearance ($Cl_{int}$) of 2.72 µL/min/mg and an average half-life of 509.4 minutes. To provide a context for dihexa's clearance rate the stability of piroxicam (60.2 µL/min/mg), verapamil (112.5 µL/min/mg) and 7-ethoxycoumarin (136.7 µL/min/mg) was also monitored as high, moderate and low metabolized standards, respectively. The clearance rates indicated above were within the published ranges for these often employed standards (Di 2003, Shou 2005, Lu 2006, Behera 2008). The clearance time courses for dihexa and the standards fit curves defining single-phase exponential decay processes with an $R^2$ values between of 0.96 and 0.99 (**Supplemental Figure 3**).

***Dihexa exhibits pro-cognitive activity***

The essential test of the success of the structural modifications incorporated into dihexa was whether it possessed pro-cognitive activity like its parent compound $Nle^1$-AngIV. Therefore, dihexa's ability to reverse scopolamine–dependent deficits in water maze performance was established. The initial study, which was simply tasked with verifying its pro-cognitive activity, entailed the direct brain delivery of dihexa via icv cannula. The data presented in **Figure 3A** confirm our expectation that dihexa would retain biological activity. Both the low and high dose groups of dihexa yielded significantly improved performance when compared to the scopolamine group from day 2 of testing on ($p<.001$). The high dose group was indistinguishable from the vehicle control group at all testing days ($p>.05$).

Since the ultimate goal of the project was to produce a clinically relevant molecule that could be delivered peripherally but still exhibit pro-cognitive/anti-dementia activity, the effectiveness of both the intraperitoneal and oral delivery routes of dihexa administration were determined using the scopolamine model. As can be seen in **Figures 3B&C**, both delivery methods yielded the anticipated biological activity. Furthermore, both studies indicated a clear dose-response relationship between the dose of dihexa and water maze performance. The high doses of each method of delivery (ip=0.5mg/kg/day; oral= 2.0 mg/kg/day) produced performances that were significantly improved over that seen in the scopolamine groups ($p<.001$) and indistinguishable from vehicle controls ($p>.05$).

Probe trials on day 9 were again employed to evaluate the strength and persistence of the learned task. As can been seen in **Figures 4A, B, &C,** dihexa at its highest dose significantly ($p<.001$) increased the time spent in the target quadrant when compared to the scopolamine impaired groups regardless of the delivery method employed and was not different from non-scopolamine treated controls ($p>.05$). In each case where multiple doses of dihexa were utilized the probe trial data yielded a dose-response relationship similar to that observed for escape latencies.

While the scopolamine model is often used to assess the cognitive enhancing capacity of experimental molecules it clearly initiates learning deficits in a non-physiological manner that only results in acute deficits. In order to begin to assess the clinical potential of dihexa as an anti-dementia drug we chose to evaluate its effects on a more physiological relevant model- the aged Sprague Dawley rat. Rats like human develop age-related cognitive difficulties. Typically about 50% of rats exhibit impaired

performance in the water maze when compared to 3 month old rats (Zeng et al., 2012). As such, we evaluated the ability of orally delivered dihexa (2mg/kg/daily) to impact water maze learning in 24 month old Sprague Dawley rats of mixed gender. As expected the results shown in **Figure 5** indicate that dihexa significantly improved performance ($p<.05$) on most of the test days. It should be noted that because these aged rats were not pre-screened for cognitive deficits the results substantially underestimate the effect of dihexa. The expectation that only half of the untreated rats would be effective learners even without dihexa treatment likely contributed to the high variability in escape latencies seen with the untreated group.

***Dihexa induces spinogenesis in cultured hippocampal neurons***

Recently the pro-cognitive effects of Nle$^{1}$-AngIV, the parent compound of dihexa, and several C-terminal truncated analogs have been correlated with their ability to induce dendritic spine formation and the establishment of new synapses (Benoist et al., 2011). As such, the influence of dihexa on spinogenesis and synaptogenesis in high density mRFP-β-actin transfected rat hippocampal neuronal cultures was evaluated. Actin-enriched spines increased in number in response to both dihexa (**Figure 6B&D**) and Nle$^{1}$-AngIV (**Figure 6C&D**) following 5 days of treatment at $10^{-12}$M concentration that started on the 7$^{th}$ day *in vitro* (DIV7) The results revealed a near 3-fold increase in the number of spines stimulated by dihexa and greater than 2-fold increase for Nle$^{1}$-AngIV. Both treatment groups differed significantly from the vehicle control group for which the average number of spines per 50 μm dendrite length was 15. The average number of spines for the dihexa and Nle$^{1}$-AngIV treated groups was 41 and 32 spines per 50 μm

dendrite length, respectively (mean ± S.E.M., n = 200 dendritic segments; *** = P < 0.001 by one-way ANOVA and Tukey post hoc test).

The icv water maze data with dihexa indicate a modest but significant improvement in spatial learning performance even on the first day of testing thus suggesting that the underlying mechanism responsible for the behavior must be rapidly engaged. Therefore the ability of both dihexa and $Nle^1$-AngIV to promote spinogenesis was assessed following an acute 30 minute application on the final day of culturing (**Figure 6E**). The acute 30 minute application of dihexa and $Nle^1$-AngIV, on the $12^{th}$ day *in vitro* (DIV12) reveals a significant increase in spines compared to 30 minute vehicle treated neurons (dihexa mean spine numbers per 50 μm dendrite length = 23.9; $Nle^1$-AngIV mean spine numbers per 50 μm dendrite length = 22.6; vehicle control treated neurons mean spine numbers per 50 μm dendrite length = 17.4; n = 60; *** = $p < 0.0001$ by one-way ANOVA followed by Tukey post-hoc test).

Strong correlations exist between spine size, persistence of spines, number of AMPA-receptors and synaptic efficacy. A correlation between the existence of long-term memories to spine head volume has also been suggested (Kasai, Fukuda et al.; Yuste and Bonhoeffer , 2001; Yasumatsu et al. 2008). With these considerations in mind spine head size measurements were taken following 5 days of drug treatment. Results indicate that the $10^{-12}$ M dose of dihexa and $Nle^1$-AngIV both increased spine head width (**Supplemental Figure 4**). The mean spine head width for $Nle^1$-AngIV was 0.87 μm, 0.80 μm for dihexa, and 0.67 μm for vehicle controls.

JPET Fast Forward. Published on October 10, 2012 as DOI: 10.1124/jpet.112.199497
This article has not been copyedited and formatted. The final version may differ from this version.



***Dihexa and Nle$^1$-AngIV Mediate Synaptogenesis***

To begin to assess the functionality of the newly formed dendritic spines, mRFP-β-actin transfected neurons were immuno-stained for three synaptic markers. Hippocampal neurons were stimulated for 5 days *in vitro* with $10^{-12}$ M dihexa or Nle$^1$-AngIV (**Figure 7**). Since glutamate synaptic transmission is known to involve receptors that reside on dendritic spines, neurons were probed for excitatory synaptic transmission by staining for the glutamatergic presynaptic marker Vesicular Glutamate Transporter 1 (VGLUT1) (Balschun et al. 2010). The universal presynaptic marker synapsin was also visualized to assess the juxtaposition of the newly formed spines with presynaptic boutons (Ferreira and Rapoport, 2002). Finally PSD-95 served as a marker for the postsynaptic density (El Husseini et al. 2000).

Again dihexa and Nle$^1$-AngIV treatment significantly augmented dendritic spinogenesis (**Figure 7 B, D, F**) in each of the three studies.; mean spine numbers for the combined studies for Nle$^1$-AngIV = 39.4; mean spine numbers for dihexa = 44.2; and, mean spine numbers for vehicle treated neurons = 23.1 (mean ± S.E.M., *** = $P < 0.001$). The percent correlation for the newly formed spines with synaptic markers VGLUT1, synapsin or PSD-95 is shown in **Figures 7 C, E, and E.** Dihexa and Nle$^1$-AngIV treatment-induced spines did not differ from control treated neurons in the percent correlation to VGLUT1, synapsin or PSD-95 ($P > 0.05$) indicating that the newly formed spines contained the same synaptic machinery as already present spines. The above results suggest that the newly formed dendritic spines produced by dihexa and Nle$^1$-AngIV treatment are creating functional synapses.

To further support this conclusion, mini postsynaptic excitatory currents (mEPSCs), the frequency of which corresponds to the number of functional synapses, were recorded from mRFP-β-actin transfected hippocampal neurons (**Figure 8**). The mean frequency of AMPA-mediated mEPSCs recorded from vehicle treated neurons was 3.06 ± 0.23 Hz from 33 cells while Nle$^1$-AngIV induced a 1.7 fold increase (5.27 ± 0.43 Hz from 25 cells; Mean ± S.E.M.; *** = $P < 0.001$ vs. control group) and dihexa produced a 1.6 fold increase (4.82 ± 0.34 Hz from 29 cells; *** = $P < 0.001$ vs. control group) confirming the expected expansion of functional synapses. No differences in amplitude, rise- or decay-times were observed (data not shown) which suggests that the individual properties of the synapse were not altered.

***Dihexa and Nle$^1$-AngIV Induce Spinogenesis in Hippocampal Organotypic Cultures***

To further assess the physiological significance of the spine induction witnessed in dissociated neonatal hippocampal neurons the effects of dihexa and Nle$^1$-AngIV on spine formation in organotypic hippocampal slice cultures was evaluated. These preparations, while still neonatal in origin, represent a more intact and three dimensional environment than dissociated neurons. Hippocampal CA1 neurons, which have been functionally linked to hippocampal plasticity and learning/memory, were easily identified based on morphological characteristics and singled out for analysis. Dihexa and Nle$^1$-AngIV significantly augmented spinogenesis in organotypic hippocampal slice cultures when compared to vehicle treated neurons. There were no differences in spine numbers between the dihexa and Nle$^1$-AngIV treatment groups (**Supplemental Figure 5**). Spine numbers measured for control slices were 7 per 50 µm dendrite length vs. 11 spines per

JPET Fast Forward. Published on October 10, 2012 as DOI: 10.1124/jpet.112.199497
This article has not been copyedited and formatted. The final version may differ from this version.



50 µm dendrite length for both Nle$^{1}$-AngIV and dihexa treated neurons; mean ± S.E.M., n = 13-20 dendritic segments; ** = $P < 0.01$.

JPET Fast Forward. Published on October 10, 2012 as DOI: 10.1124/jpet.112.199497
This article has not been copyedited and formatted. The final version may differ from this version.



## DISCUSSION

The goal of this study was to develop an AngIV-derived molecule that retained the pro-cognitive/anti-dementia activity of AngIV and Nle$^1$-AngIV but possessed improved pharmacokinetic properties, thus allowing it to penetrate the BBB in sufficient quantities to reach therapeutic levels in the brain. The culmination of this effort was dihexa, a hydrophobic, N- and C-terminal modified, AngIV-related peptide. The cursory pharmacokinetic characterization of dihexa included in this study indicated that it was stable in serum, had a long circulating half-life, and penetrated the BBB. Data from behavioral studies using scopolamine amnesia and aged rat models, where dihexa was able to reverse cognitive deficits, indicated that the metabolic stability and BBB permeability of dihexa was apparently high enough to attain therapeutic brain levels after oral administration. Additional mechanistic studies demonstrated that both dihexa and Nle$^1$-AngIV, its parent compound, were effective stimulators of hippocampal synaptogenesis thus providing a rational explanation for their pro-cognitive activities.

The starting point for this study was a recently published study (Benoist et al., 2011) that determined that the information in Nle$^1$-AngIV critical to its pro-cognitive activity resided in its three to four N-terminal amino acids. Using the N-terminal tripeptide of Nle$^1$-AngIV as a starting point the intermediate goal of this study was to establish the impact of various N- and C-terminal modifications of peptide stability. The results indicated that N-terminal modifications were particularly effective at enhancing metabolic stability; while C-terminal amidation offered more modest protection. The observation that replacement of the N-terminal norleucine with GABA yielded a compound with superior anti-dementia activity indicated that an N-terminal $\alpha$-amino

group was not required for activity. Furthermore, these data suggested that N-terminal, N-acyl tyrosine containing tripeptides should be biologically active. This observation, coupled with the added stability contributed by C-terminal amidation and the desire to increase the hydrophobicity of the peptide, led to the generation of a series of compounds with the structure, N-acyl-Tyr-Ile-(6) amino-hexanoic amide. After preliminary functional screening (see below), N-hexanoic-Tyr-Ile-(6)amino-hexanoic amide was chosen for further investigation with the expectation that it would be biologically active, metabolically stable, and BBB permeable.

Although not the focus of this study an obvious question relates to the identity of the molecular target responsible for the pro-cognitive and synaptogenic activity of dihexa and other AngIV-related compounds. Hints to the answer to this question can be found in four recent articles (Yamamoto et al., 2010; Kawas et al., 2011; Kawas et al., 2012, Wright et al., 2012), which clearly demonstrate that both the peripheral and CNS actions of "$AT_4$ receptor" antagonists depend on their ability to inhibit the hepatocyte growth factor (HGF)/ c-Met (HGF receptor) system by binding to and blocking HGF activation. Conversely we (Benoist, Kawas, Wright, and Harding unpublished) have recently demonstrated that both $Nle^1$-AngIV and dihexa bind HGF leading to its activation and that the pro-cognitive and/or synaptogenic actions of these compounds are blocked by both HGF and c-Met antagonists. With this knowledge in hand a library of N-acyl-Tyr-Ile-(6) amino-hexanoic amide analogs was screened for their capacity to potentiate the biological activity of HGF. This screen identified the hexanoic N-terminal substituent as the most active compound.

The ultimate goal of this project was to produce a clinically useful pharmaceutical for the treatment of dementia including Alzheimer's disease. At its core dementia results from a combination of diminished synaptic connectivity among neurons and neuronal death in the entorhinal cortex, hippocampus and neocortex. Therefore, an effective treatment would be expected to augment synaptic connectivity, protect neurons from underlying death inducers, and stimulate the replacement of lost neurons from preexisting pools of neural stem cells. These clinical endpoints advocate for the therapeutic use of neurotrophic factors, which mediate neural development, neurogenesis, neuroprotection, and synaptogenesis. Not unexpectedly neurotrophic factors have been considered as treatment options for many neurodegenerative diseases including Alzheimer's disease (see reviews-Nagahara et al., 2011; Calissano et al., 2010). The realization that activation of the HGF/c-Met system represents a viable treatment option for dementia should be no surprise. HGF is a potent neurotrophic factor in many brain regions (Kato et al., 2009; Ebens et al., 1996), while affecting a variety of neuronal cell types. However, the direct use of HGF or any other protein neurotrophic factor as a therapeutic agent has two serious limitations: 1) large size and hydrophilic character precludes BBB permeability; and 2) the need to be manufactured by recombinant methods at high cost, thus limiting its widespread use. The development of Dihexa has seemingly overcome these impediments by virtue of its oral activity, demonstrated pro-cognitive/anti-dementia activity, and anticipated low manufacturing costs. Among planned future studies, designed to gage the clinical potential of dihexa, will be a direct comparison of dihexa to several approved anti-dementia therapeutics using rodent dementia models.

## AUTHORSHIP CONTRIBUTION

*Participated in research design:* McCoy, Benoist, Wright, Harding, Appleyard, Wayman, Kawas

*Provided specialty chemicals or reagents:* Harding

*Conducted experiments:* McCoy, Benoist, Zhu, Kawas, Bule-Ghogare, Zhu, Wright

*Performed data analysis:* McCoy, Harding, Benoist, Kawas, Wright, Bule-Ghogare, Zhu

*Wrote or contributed to the writing of the manuscript:* McCoy, Benoist, Wright, Kawas, Bule, Appleyard, Wayman, Harding

## REFERENCES

Abhold RH and Harding JW (1988) Metabolism of angiotensins II and III by membrane-bound peptidases from rat brain. *J Pharmacol Exp Ther* **245**:171-177.

Balschun D, Moechars D, Callaerts-Vegh Z, Vermaercke B, Van Acker N, and Andries L, D'Hooge R (2010) Vesicular glutamate transporter VGLUT1 has a role in hippocampal long-term potentiation and spatial reversal learning. *Cereb Cortex* **20**:684-693.

Behera D, Damre A, Varghese A, and Addepalli V (2008) In vitro evaluation of hepatic and extra-hepatic metabolism of coumarins using rat subcellular fractions: correlation of in vitro clearance with in vivo data. *Drug Metabolism and Drug Interactions* **23**:329-350.

Benoist CC, Wright JW, Zhu M, Appleyard SM, Wayman GA, and Harding JW (2011) Facilitation of hippocampal synaptogenesis and spatial memory by C-terminal truncated Nle1-angiotensin IV analogs. *J Pharmacol Exp Ther* **339**:35-44.

Braszko JJ, Kupryszewski G, Witczuk B, and Wisniewski K (1988) Angiotensin II-(3-8)-hexapeptide affects motor activity, performance of passive avoidance and a conditioned avoidance response in rats. *Neuroscience* **27**:777-783.

Calissano P, Matrone C, and Amadoro G (2010) Nerve growth factor as a paradigm of neurotrophins related to Alzheimer's disease. *Dev Neurobiol* **70**:372-383

De Bundel D, Smolders I, Vanderheyden P and Michotte Y (2008) Ang II and Ang IV: unraveling the mechanism of action on synaptic plasticity, memory, and epilepsy. *CNS Neurosci Ther* **14**:315-339.

Dewey AL, Wright JW, Hanesworth JM, and Harding JW (1988) Effects of aminopeptidase inhibition on the half-lives of [125I]angiotensins in the cerebroventricles of the rat. *Brain Research* **448**:369-72.

Di L, Kerns EH, Gao N, Li SQ, Huang Y, Bourassa JL, and Huryn DM (2004) Experimental design on single-time-point high-throughput microsomal stability assay. *J Pharmaceut Sci* **93**:1537-1544.

Ebens A, Brose K, Leonardo ED, Hanson MG, Jr., Bladt F, Birchmeier C, Barres BA and Tessier-Lavigne M (1996) Hepatocyte growth factor/scatter factor is an axonal chemoattractant and a neurotrophic factor for spinal motor neurons. *Neuron* **17**:1157-1172.

El-Husseini AE, Schnell E, Chetkovich DM, Nicoll RA, and Bredt DS (2000) PSD-95 involvement in maturation of excitatory synapses. *Science* **290**: 1364-1368.

Faure S, Chapot R, Tallet D, Javellaud J, Achard JM and Oudart N (2006) Cerebroprotective effect of angiotensin IV in experimental ischemic stroke in the rat mediated by AT(4) receptors. *J Physiol Pharmacol* **57**:329-342.

Ferreira A and Rapoport M (2002) The synapsins: beyond the regulation of neurotransmitter release. *Cell Mol Life Sci* **59**:589-595.

Fisher A, Pittel Z, Haring R, Bar-Ner N, Kliger-Spatz M, Natan N, Egozi I, Sonego H, Marcovitch I and Brandeis R (2003) M1 muscarinic agonists can modulate some of the hallmarks in Alzheimer's disease: implications in future therapy. *J Mol Neurosci* **20**:349-356.

Gard PR (2004) Angiotensin as a target for the treatment of Alzheimer's disease, anxiety and depression. *Expert Opin Ther Targets* **8**:7-14.

Gard PR (2008) Cognitive-enhancing effects of angiotensin IV. *BMC Neurosci* **9 Suppl 2**:S15.

Kasai H, Fukuda M, Watanabe S, Hayashi-Takagi A and Noguchi (2010) J Structural dynamics of dendritic spines in memory and cognition. *Trends Neurosci* **33**:121-129.

Kato N, Nemoto K and Nakanishi K (2009) Efficacy of HGF gene transfer for various nervous injuries and disorders. *Cent Nerv Syst Agents Med Chem* **9**:300-306.

Kawas LH, McCoy AT, Yamamoto BJ, Wright JW and Harding JW (2012) Development of Angiotensin IV Analogs as Hepatocyte Growth Factor/Met Modifiers. *J Pharmacol Exp Ther* **340**:539-548.

Kawas LH, Yamamoto BJ, Wright JW and Harding JW (2011) Mimics of the dimerization domain of hepatocyte growth factor exhibit anti-met and anti-cancer activity. *J Pharmacol Exp Ther* **339**:509-518.

Kramar EA, Armstrong DL, Ikeda S, Wayner MJ, Harding JW and Wright JW (2001) The effects of angiotensin IV analogs on long-term potentiation within the CA1 region of the hippocampus in vitro. *Brain Res* **897**:114-121.

Kramar EA, Harding JW and Wright JW (1997) Angiotensin II- and IV-induced changes in cerebral blood flow. Roles of AT1, AT2, and AT4 receptor subtypes. *Regul Pept* **68**:131-138.

Krebs LT, Kramár EA, Hanesworth JM, Sardinia MF, Ball AE, Wright JW, and Harding JW (1996) Characterization of the binding properties and physiological action of divalinal-angiotensin IV, a putative AT4 receptor antagonist. *Regul Pept* **3**:123-30.

Lee J, Albiston AL, Allen AM, Mendelsohn FA, Ping SE, Barrett GL, Murphy M, Morris MJ, McDowall SG and Chai SY (2004) Effect of I.C.V. injection of AT4 receptor ligands, NLE1-angiotensin IV and LVV-hemorphin 7, on spatial learning in rats. *Neuroscience* **124**:341-349.

Lu C, Li P, Gallegos R, Uttamsingh V, Xia CQ, Miwa GT, Balani SK, and Gan L (2006) Comparison of intrinsic clearance in liver microsomes and hepatocytes from rats and humans: evaluation of free fraction and uptake in hepatocytes. *Drug Metab Disposition* **34**:1600-1605.

Meijering E, Jacob M, Sarria JC, Steiner P, Hirling H and Unser M (2004) Design and validation of a tool for neurite tracing and analysis in fluorescence microscopy images. *Cytometry A* **58**:167-176.

Mustafa T, Lee JH, Chai SY, Albiston AL, McDowall SG and Mendelsohn FA (2001) Bioactive angiotensin peptides: focus on angiotensin IV. *J Renin Angiotensin Aldosterone Syst* **2**:205-210.

Nagahara AH and Tuszynski MH (2011) Potential therapeutic uses of BDNF in neurological and psychiatric disorders. *Nat Rev Drug Discov* **10**:209-219.

Pederson ES, Krishnan R, Harding JW and Wright JW (2001) A role for the angiotensin AT4 receptor subtype in overcoming scopolamine-induced spatial memory deficits. *Regul Pept* **102**:147-156.

Shou WZ, Magis L, Li AC, Naidong W, and Bryant MS (2005) A novel approach to perform metabolite screening during the quantitative LC-MS/MS analyses of in vitro metabolic stability samples using a hybrid triple-quadrupole linear ion trap mass spectrometer. *J Mass Spectrometry* **40**:1347-1356

Stubley-Weatherly L, Harding JW and Wright JW (1996) Effects of discrete kainic acid-induced hippocampal lesions on spatial and contextual learning and memory in rats. *Brain Res* **716**:29-38.

von Bohlen und Halbach O (2003) Angiotensin IV in the central nervous system. *Cell Tissue Res* **311**:1-9.

Wayman GA, Davare M, Ando H, Fortin D, Varlamova O, Cheng HY, Marks D, Obrietan K, Soderling TR, Goodman RH and Impey S (2008) An activity-regulated microRNA controls dendritic plasticity by down-regulating p250GAP. *Proc Natl Acad Sci U S A* **105**:9093-9098.

Wayman GA, Impey S, Marks D, Saneyoshi T, Grant WF, Derkach V, Soderling TR. (2006) Activity-dependent dendritic arborization mediated by CaM-kinase I activation and enhanced CREB-dependent transcription of Wnt-2. *Neuron* **50**:897-909.

Wright JW, Clemens JA, Panetta JA, Smalstig EB, Weatherly LA, Kramar EA, Pederson ES, Mungall BH, and Harding JW (1996) Effects of LY231617 and angiotensin

IV on ischemia-induced deficits in circular water maze and passive avoidance performance in rats. *Brain Res* **717**:1-11.

Wright JW, and Harding JW (2008) The brain RAS and Alzheimer's disease. *Exp Neurol* **223**:326-333.

Wright JW, Morseth SL, Abhold RH, and Harding JW (1985) Pressor action and dipsogenicity induced by angiotensin II and III in rats. Am J Physiol 249:R514-521.

Wright JW, Stubley L, Pederson ES, Kramar EA, Hanesworth JM and Harding JW (1999) Contributions of the brain angiotensin IV-AT4 receptor subtype system to spatial learning. *J Neurosci* **19**:3952-3961.

Wright JW, Wilson WL, Wakeling V, Boydstun AS, Jensen, A, Kawas, LH, and Harding JW (2012) The Angiotensin IV Analogue and Hepatocyte Growth Factor/ c-Met Antagonist, Divalinal-AngIV, Attenuates the Acquisition of Methamphetamine-Dependent Condition Place Preference in Rats. *Brain Sci* 2:298-318.

Yamamoto BJ, Elias PD, Masino JA, Hudson BD, McCoy AT, Anderson ZJ, Varnum MD, Sardinia MF, Wright JW and Harding JW (2010) The Angiotensin IV Analog Nle-Tyr-Leu-Ψ-(CH2-NH2)3-4-His-Pro-Phe (Norleual) Can Act as a Hepatocyte Growth Factor/c-Met Inhibitor. *J Pharmacol Exp Ther* **333**:161-173.

Yasumatsu, N., Matsuzaki M, Noguchi J, and Kasai H (2008). "Principles of long-term dynamics of dendritic spines." J Neurosci **28**: 13592-608.

Yuste, R. and Bonhoeffer T (2001) Morphological changes in dendritic spines associated with long-term synaptic plasticity *Annu Rev Neurosci* **24**: 1071-89.

## FOOTNOTES

a) Alene McCoy, Caroline Benoist, and John Wright contributed equally to the generation and presentation of the data described in this study.

b) The studies described were supported by the Edward E. and Lucille I. Lainge Endowment for Alzheimer's Research and funds provided for medical and biological research by the State of Washington Initiative Measure No. 171 to JWW and NIH grant [MH086032] and a Hope for Depression Research Foundation grant to GAW.

c) JWW and JWH are founders and shareholders in $M^3$ Biotechnology, LLC, which is developing pharmaceuticals based on this technology.

d) An abstract of part of this work has appeared [Caroline C. Benoist, John W. Wright, Mingyan Zhu, Leen H. Kawas, Suzanne A. Appleyard, Gary A. Wayman, Joseph W. Harding: Evaluation of an Orally Active Angiotensin IV Analogue; Society for Neuroscience Meeting (2010) Abstract # 856.3]

## LEGENDS FOR FIGURES

**Figure 1: Metabolically stabilized AngIV analogs reverse scopolamine-dependent spatial learning deficits. A.** Group latencies to find the submerged platform in the Morris water maze task of spatial memory. Data from six groups of rats (N=8 each) that were pretreated with icv scopolamine (70 nmol in 2 µl aCSF) 20 min prior to training followed by the icv infusion of the designated analog (1 nmol in 2 µl aCSF) 5 min prior to daily training are shown. A two-way ANOVA with repeated measures indicated that all groups were different from the scopolamine►aCSF on at the last five days of testing. Mean±SEM; ***$p < 0.001$. **B.** Day 9 probe trials by each experimental group. Time spent in the target quadrant was recorded for each experimental group. All treatment groups were different from the scopolamine►aCSF group (**$p<.01$) but not significantly different from the vehicle group ($p>.05$). The GABA-Tyr-Ile group was also different than all the other treated groups (*$p<.05$). aCSF= artificial cerebrospinal fluid.

**Figure 2: Dihexa is concentrated in multiple brain regions.** Rats fitted with a carotid cannula were anesthetized and infused with 0.5ml of isotonic saline containing 10µCi of $^{3}$H-dihexa and 2µCi $^{14}$C-Inulin, a vascular marker. Thirty minutes after infusion the rats were decapitated, the brains removed, and various brain regions dissected. The tissues were then weighed and solubilized with NCS, an organic protein solubilizing agent, and 10ml of scintillation was added. Samples were counted with a scintillation counter using two different windows to quantitate both $^{3}$H and $^{14}$C counts. $^{3}$H /$^{14}$C ratios were determined so that blood derived dihexa contamination of tissues could be determined. The results indicate that all brain regions concentrated dihexa (***$p<.001$) when

compared to blood but no area was statistically different from any other (p>.05).The average $^{3}H$ /$^{14}C$ for blood was 1687. Mean+/-S.E.M.; n=4.

**Figure 3: Dihexa reverses scopolamine-dependent spatial learning deficits.** Group latencies to find the submerged platform in the Morris water maze task of spatial memory are shown. 20 minutes before beginning testing 3 month old male Sprague Dawley rats were given scopolamine directly into the brain (icv) and 15 minutes later dihexa was given either icv, intraperitoneally (ip), or orally. There were 5 trials per day for 8 days. The latency to find the pedestal was considered a measure of learning and memory. **A.** Rats were pretreated with icv scopolamine (70 nmol in 2 µl aCSF) 20 min prior to training followed by the icv infusion of dihexa (0.1 or 1 nmol in 2 µl aCSF) 5 min prior to daily training. A two-way ANOVA with repeated measures indicated that all time points for the 1nmol dihexa group were different from the scopolamine group, which received vehicle (aCSF) instead of dihexa (***p<.001). The lower, 0.1nmol, dose of dihexa was also significantly improved performance when compared to the scopolamine group on days 5-8 of testing (*p<.05). **B.** Rats were pretreated with icv scopolamine (70 nmol in 2 µl aCSF) 20 min prior to training followed 15 minutes later by an ip injection of dihexa in DMSO (<1%) at .05mg/kg, .25mg/kg, or .50mg/kg. A two-way ANOVA with repeated measures indicated that the latency curves for dihexa at .25mg/kg and .50mg/kg were different than the scopolamine►aCSF group's learning curve (***p<.001). The .50mg/kg group was not different than the vehicle control group (p>.05) while the .05mg/kg dihexa group was not different than the scopolamine group (p>.05). **C.** Rats were pretreated with icv scopolamine (70 nmol in 2 µl aCSF) 20 min prior to training followed by oral delivery (gavage) of dihexa at 1.25/kg and 2.0mg/kg

.25mg/kg (suspension in isotonic NaCl), 5 min prior to daily training. The high oral (2 mg/kg) dose of dihexa completely reversed the scopolamine-dependent learning deficit (***p<.001) while the effect of scopolamine was partially reversed at the 1.25 kg/mg dose on days 3-8 (p<.01). aCSF= artificial cerebrospinal fluid. Mean +/-SEM; n=8-10

**Figure 4: Dihexa increases time in the target quadrant during day 9 probe trials.** Time spent in the target quadrant was recorded for each experimental group following icv, ip, and oral delivery of dihexa. **A.** In the icv study the scopolamine group performed below the chance level (30s) and was significantly different from the vehicle control group and the scopolamine►dihexa 1nmol group (***p<.001) while the scopolamine►dihexa 1nmol and vehicle control groups were not different (p>.05). **B.** In the ip. delivery study the scopolamine►PBS group preformed below the chance level and was different than the vehicle control group (***p<.001). Each of the treatment groups was different than the scopolamine►PBS group (***p<.001-*p<.05) while each of the treatment groups was different than one another (***p<.001-*p<.05) exhibiting the same dose-response relationship observed in the initial water maze study (Figure 3). **C.** In the oral delivery study the scopolamine►PBS group preformed near the chance level and was different than the vehicle control group (***p<.001). Both of the treatment groups were different than the scopolamine►PBS group (*p<.05 and ***p<.001 respectively) while both of the treatment groups were different from one another (***p<.001) exhibiting the same dose-response relationship observed in the initial water maze study (Figure 3). Mean+/-S.E.M.; n=8-10.

**Figure 5: Dihexa improves spatial learning in aged rats.** Group latencies to find the submerged platform in the Morris water maze task of spatial memory are shown. Five minutes before beginning testing 24 month old mixed sex (3 male and 3 female/group) Sprague Dawley rats were administered dihexa (2 mg/kg) orally by gavage (suspension in isotonic NaCl), on a daily basis. There were 5 trials per day for 8 days. The latency to find the pedestal was considered a measure of learning and memory. The learning curve for the treated rats was significantly different than that of the non-treated rats (Mann-Whitney U, *p<.03). Mean+/-S.E.M.; n=6.

**Figure 6: Nle$^{1}$-AngIV and Dihexa increase the number of dendritic spines.** Time dependent effects of Nle$^{1}$-AngIV and dihexa treated neurons on spinogenesis. Hippocampal neurons transfected with mRFP-β-actin were treated with $10^{-12}$ M dihexa or $10^{-12}$ M Nle$^{1}$-Ang IV for 5 days or 30 minutes in culture prior to fixation on day *in vitro* 12 (DIV12) . **A)** Representative image of the dendritic arbor of a 5 day vehicle treated hippocampal neuron. **B)** Representative image of a dendritic arbor from a neuron stimulated for 5 days with $10^{-12}$ M dihexa. **C)** Representative image of the dendritic arbor of a neuron stimulated with $10^{-12}$ M Nle$^{1}$-Ang IV for 5 days. **D)** Bar graph representing the number of spines per 50 µm dendrite length per treatment condition following a 5 day *in vitro* treatment. ***p < 0.001; n = 200 dendritic segments. **E)** Bar graph representing the number of spines per 50 µm dendrite length per treatment condition following an acute 30 minute treatment. ***p < 0.001; n = 60 dendritic segments. Mean ± S.E.M. Analysis by one-way ANOVA and Tukey post hoc test.

JPET Fast Forward. Published on October 10, 2012 as DOI: 10.1124/jpet.112.199497
This article has not been copyedited and formatted. The final version may differ from this version.



**Figure 7: Localization of synaptic markers following Nle$^1$-AngIV and dihexa-dependent dendritic spine induction.** Dihexa and Nle$^1$-AngIV treated neurons were immunostained for the universal presynaptic marker synapsin, the glutamatergic presynaptic marker VGLUT1, and the postsynaptic density maker PSD-95. The percent correlation between the postsynaptic spines (red) and presynaptic puncta (green), which represented a different marker in each panel, was determined and used as an indicator of functional synapses. **A)** Representative images of hippocampal neurons transfected with mRFP-β-actin and immunostained for the excitatory presynaptic marker VGLUT1, the general presynaptic marker synapsin, and the postsynaptic marker PSD-95 following a 5 day treatment with vehicle, $10^{-12}$ M Nle$^1$-AngIV or $10^{-12}$ M dihexa. **B)** Bar graph confirming the expected increase in the number of dendritic spines following treatment with vehicle, Nle$^1$-AngIV or dihexa (***$p < 0.001$; mean ± S.E.M.; n = 25 dendritic segments). **C)** Bar graph showing the percent correlation between dendritic spines after treatment and the glutamatergic presynaptic marker VGLUT1. No significant differences between the stimulated neurons and vehicle control treated neurons were observed ($P > 0.05$; mean ± S.E.M.; n = 25 dendritic segmnets). **D)** Bar graph confirming the expected increase in the number of dendritic spines following treatment with vehicle, Nle$^1$-AngIV or dihexa (***$p < 0.001$; mean ± S.E.M.; n = 25 dendritic segments). **E).** Bar graph showing the percent correlation between dendritic spines after treatment and the general presynaptic marker synapsin. No significant differences between the stimulated neurons and vehicle control treated neurons were observed ($p > 0.05$; mean ± S.E.M.; n = 25 dendritic segments). **F)** Bar graph confirming the expected increase in the number of dendritic spines following treatment with vehicle, Nle$^1$-AngIV or dihexa (***$p < 0.001$;

mean ± S.E.M.; n = 25 dendritic segments). **G)** Bar graph showing the percent correlation between dendritic spines after treatment and the postsynaptic marker PSD-95. No significant differences between the stimulated neurons and vehicle control treated neurons were observed ($p > 0.05$; mean ± S.E.M.; n = 25 dendritic segments). Together these data indicate that dendritic spines formed after treatment support functional synapses.

**Figure 8**: **Increased frequencies of mini-excitatory postsynaptic currents (mEPSCs) in dissociated hippocampal neurons treated with Nle$^{1}$-AngIV and dihexa.** Recordings were carried out on rat dissociated hippocampal neurons treated with vehicle, $10^{-12}$ M Nle$^{1}$-AngIV or $10^{-12}$ M dihexa for 5 days prior to recording. The post-synaptic currents, which were recorded in the presence of strychnine, picrotoxin and tetrodotoxin, represented spontaneous bursts likely mediated by AMPA receptors. **A)** Representative traces of mEPSC recordings from Nle$^{1}$-AngIV or dihexa treated hippocampal neurons. **B)** Bar graph illustrating the increase in mEPSC frequencies in hippocampal neurons that resulted from Nle$^{1}$-AngIV or dihexa treatment. The increased frequencies indicate that dendritic spines induced by Nle$^{1}$-AngIV or dihexa support functional synaptic transmission. *** $p < 0.001$; ± S.E.M.; n = 25.

JPET Fast Forward. Published on October 10, 2012 as DOI: 10.1124/jpet.112.199497
This article has not been copyedited and formatted. The final version may differ from this version.



## TABLES

**Table 1. Blood collection schedule following intravenous and intraperitoneal administration of dihexa.**

| Dosage Route | Dose | Blood Sample Volume | Sample Collection Times (minutes unless otherwise noted) |
|---|---|---|---|
| Intravenous | 10 mg/kg | 200 µL | 0, 10, 30, 90, 150, 240, 330, 420, 510, 600, 690, 780, 24 hours, 48 hours, 5 days |
| Intraperitoneal | 20 mg/kg | 200 µL | 0, 10, 30, 60, 90, 120, 150, 180, 240, 300, 360, 420, 480, 600, 720, 24 hours, 48 hours, 5 days |

JPET Fast Forward. Published on October 10, 2012 as DOI: 10.1124/jpet.112.199497
This article has not been copyedited and formatted. The final version may differ from this version.



**Table 2. Serum Stability of AngIV Analogs**

| Compound | Half-Life (min) |
|---|---|
| **Nle$^{1}$-AngIV** | 1.42 $^{+}$/- .26 |
| **N-acetyl-Nle-Tyr-Ile-His** | 115 $^{+}$/- 7.6 |
| **D-Nle-Tyr-Ile** | 225 $^{+}$/- 23.7 |
| **GABA-Tyr-Ile** | 946 $^{+}$/- 234 |
| **Nle-Tyr-Ile-His-$NH_2$** | 23.0 $^{+}$/- 3.1 |
| **Dihexa** | 335.5 $^{+}$/- 9.5 |

Mean $^{+}$/- SD, N = 3

JPET Fast Forward. Published on October 10, 2012 as DOI: 10.1124/jpet.112.199497
This article has not been copyedited and formatted. The final version may differ from this version.



**Table 3. Dihexa Pharmacological Parameters**

| Pharmacokinetic Parameter | Mean | ± | SEM |
|---|---|---|---|
| **$AUC_{0-\infty}$ (min.µg/mL)** | 4471 | ± | 1408 |
| **Vd (L/kg)** | 54.4 | ± | 14.8 |
| **$C_p^0$ (µg/mL)** | 87.3 | ± | 31.9 |
| **$t_{1/2}$ (min)** | 18256 | ± | 7787 |
| **KE ($min^{-1}$)** | 0.00007 | ± | 0.00004 |
| **CL (L/min/kg)** | 0.0026 | ± | 0.0007 |

N=3

JPET Fast Forward. Published on October 10, 2012 as DOI: 10.1124/jpet.112.199497
This article has not been copyedited and formatted. The final version may differ from this version.



**Table 4. Predicted Physicochemical Properties of Dihexa**

| Physicochemical Property | Predicted Value |
|---|---|
| **logP** | 2.25 |
| **$P_{eff}$** | 1.78 |
| **$P_{avg}$** | 0.62 |
| **$Pr_{Unbnd}$** | 22.59 |

JPET Fast Forward. Published on October 10, 2012 as DOI: 10.1124/jpet.112.199497
This article has not been copyedited and formatted. The final version may differ from this version.

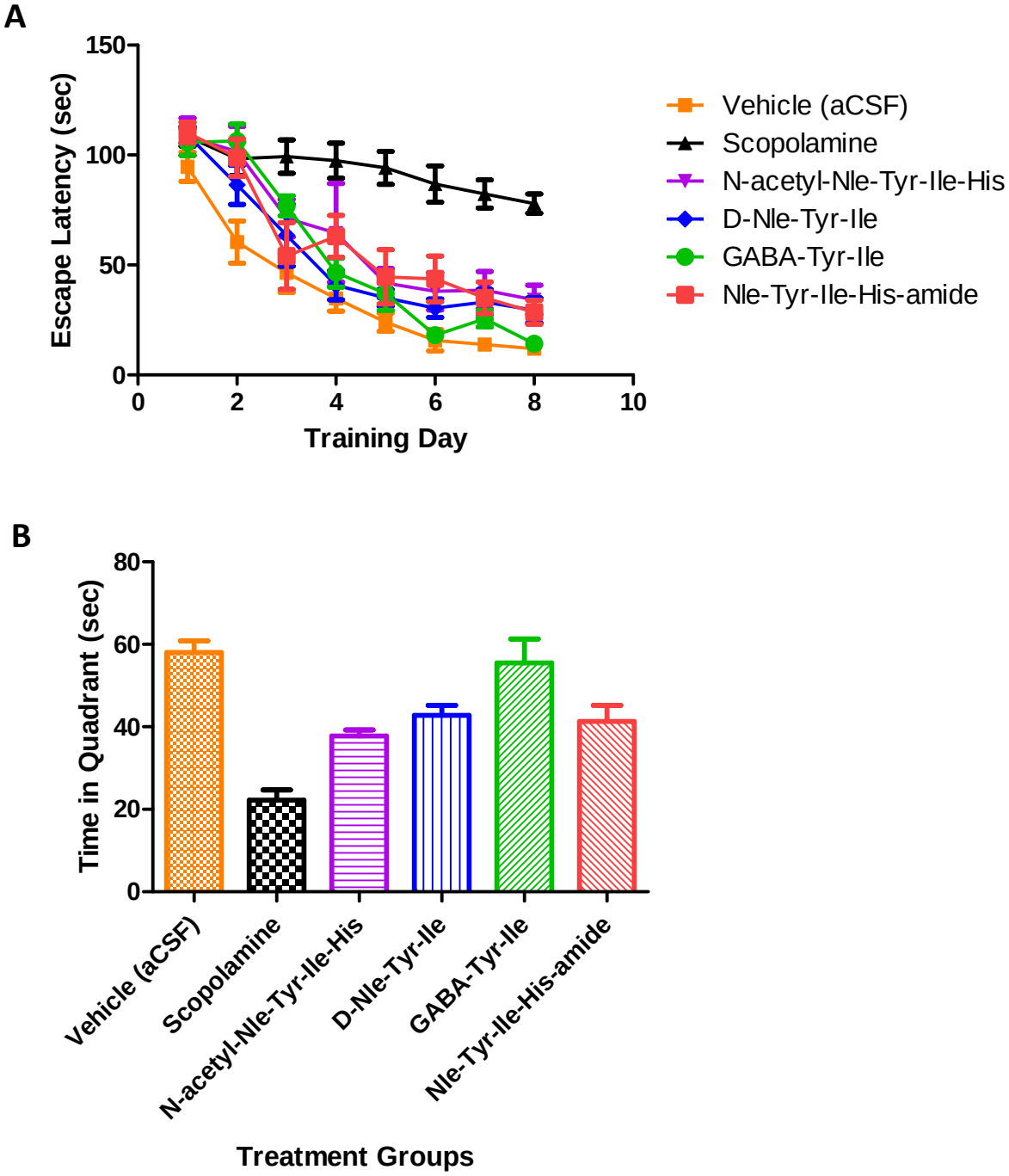


**Figure 1**

JPET Fast Forward. Published on October 10, 2012 as DOI: 10.1124/jpet.112.199497
This article has not been copyedited and formatted. The final version may differ from this version.

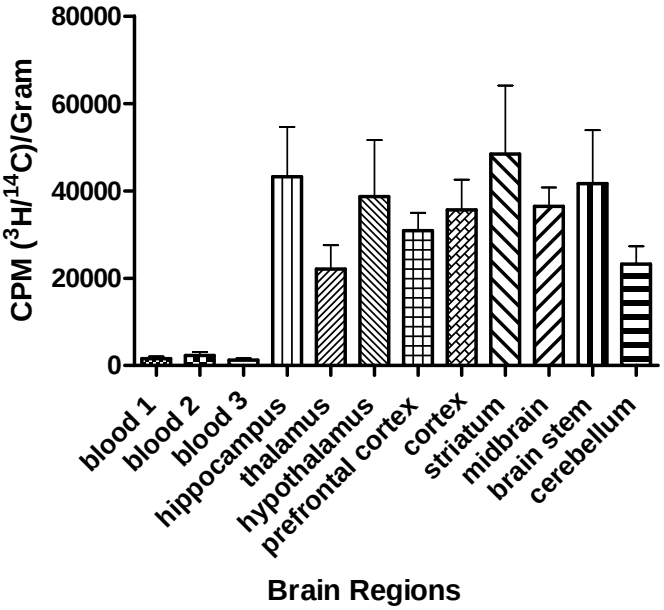


**Figure 2**

JPET Fast Forward. Published on October 10, 2012 as DOI: 10.1124/jpet.112.199497
This article has not been copyedited and formatted. The final version may differ from this version.

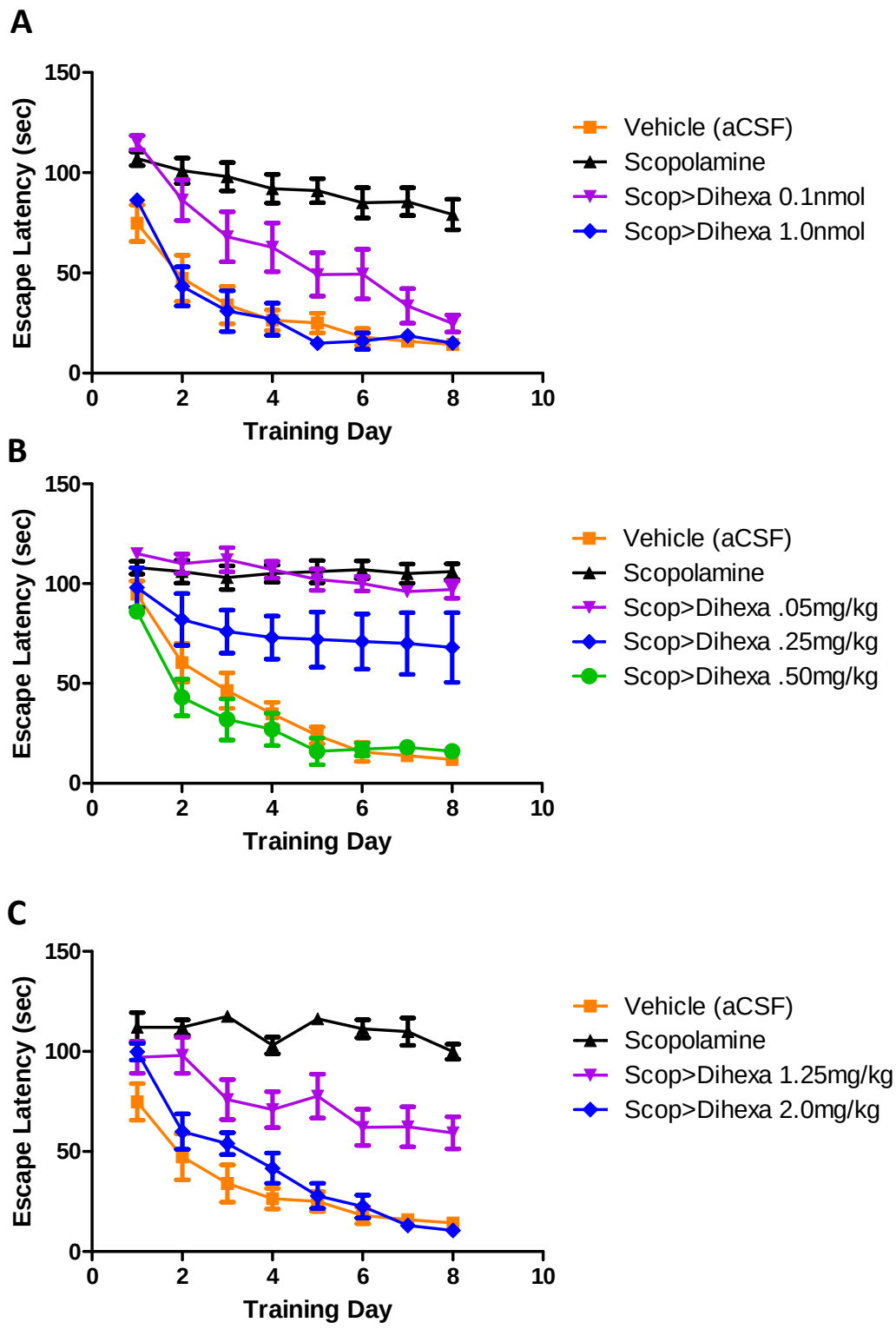


**Figure 3**

JPET Fast Forward. Published on October 10, 2012 as DOI: 10.1124/jpet.112.199497
This article has not been copyedited and formatted. The final version may differ from this version.

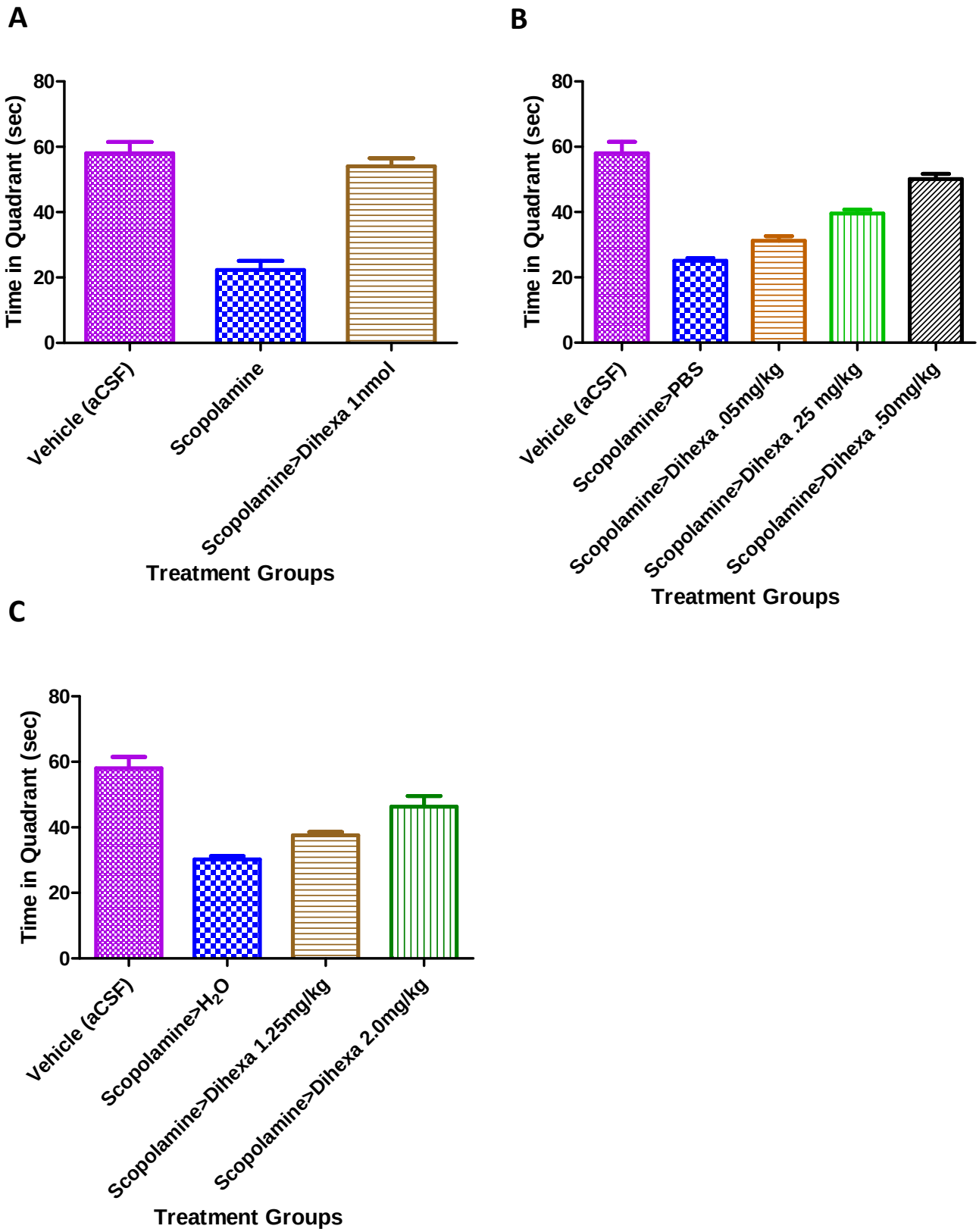


**Figure 4**

JPET Fast Forward. Published on October 10, 2012 as DOI: 10.1124/jpet.112.199497
This article has not been copyedited and formatted. The final version may differ from this version.

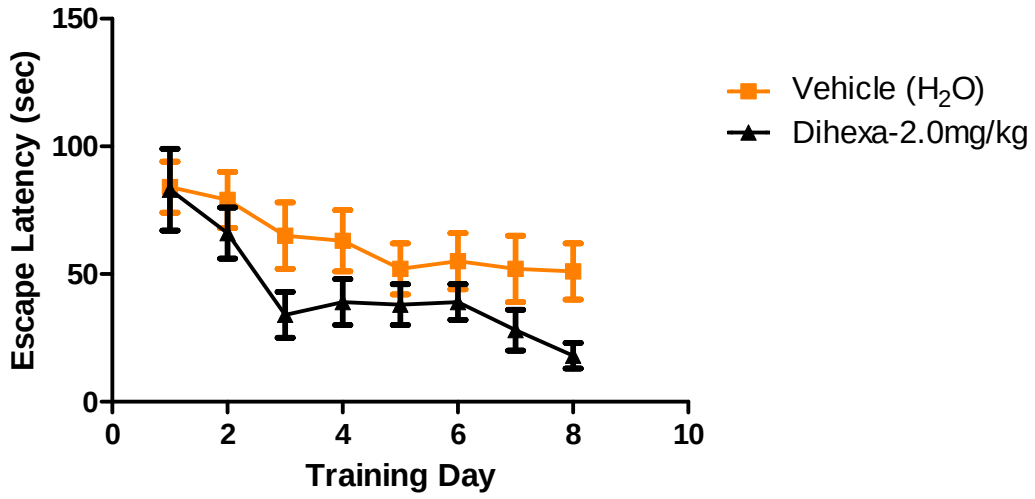


**Figure 5**

JPET Fast Forward. Published on October 10, 2012 as DOI: 10.1124/jpet.112.199497
This article has not been copyedited and formatted. The final version may differ from this version.

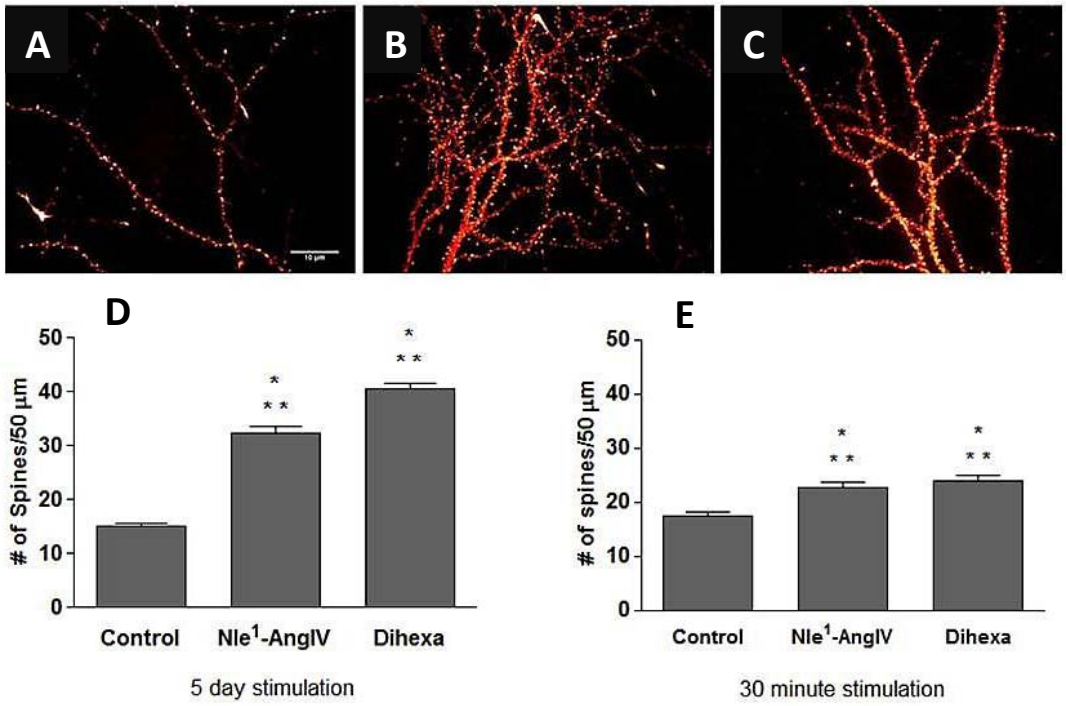


**Figure 6**

JPET Fast Forward. Published on October 10, 2012 as DOI: 10.1124/jpet.112.199497
This article has not been copyedited and formatted. The final version may differ from this version.

**A**

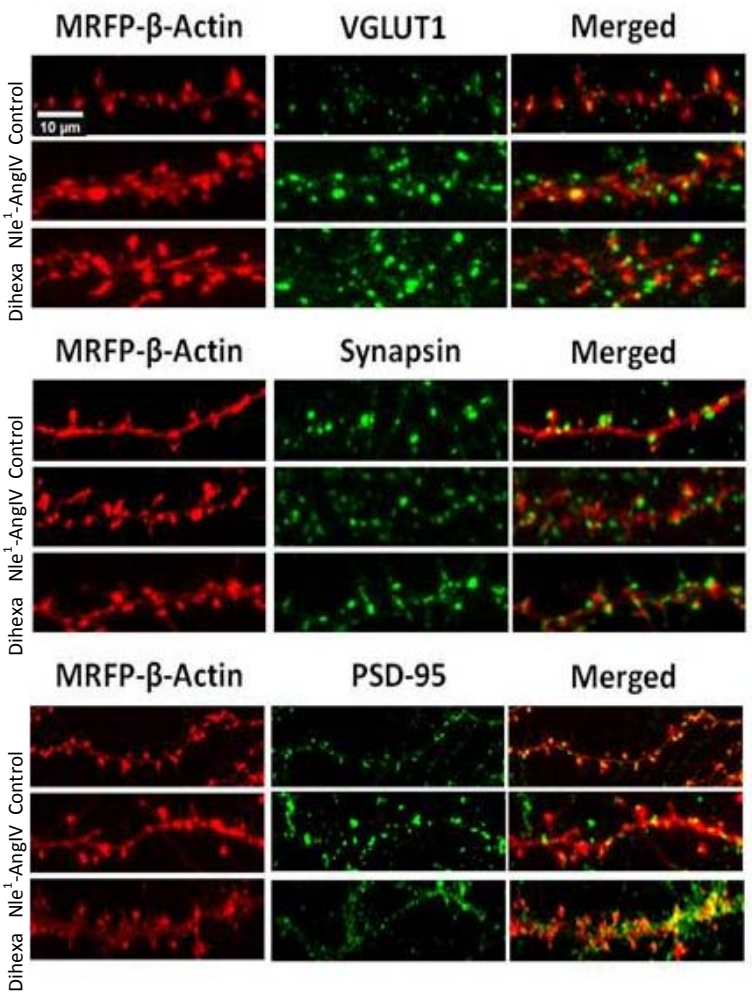


**Figure 7-1**

JPET Fast Forward. Published on October 10, 2012 as DOI: 10.1124/jpet.112.199497
This article has not been copyedited and formatted. The final version may differ from this version.

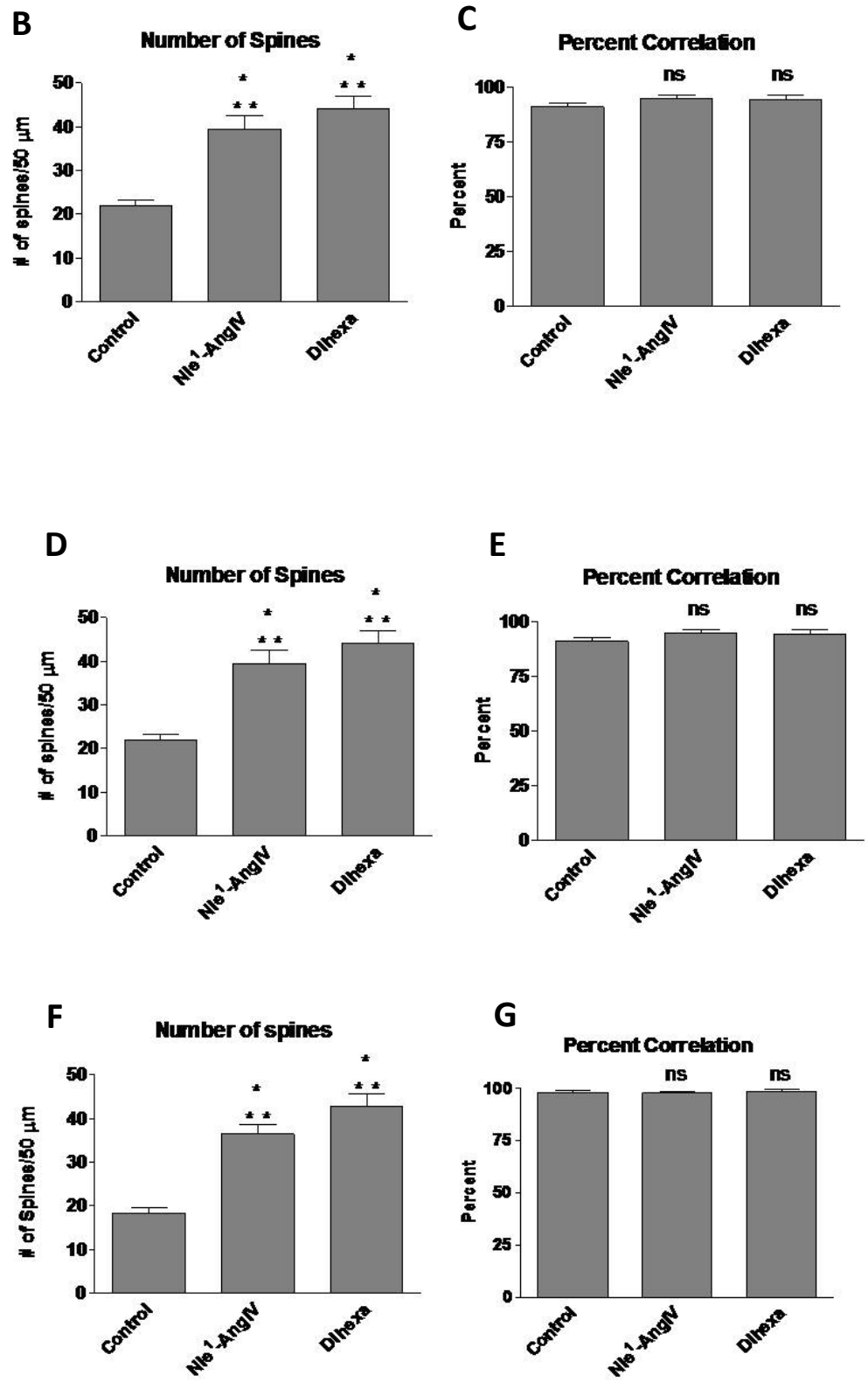


**Figure 7-2**

JPET Fast Forward. Published on October 10, 2012 as DOI: 10.1124/jpet.112.199497
This article has not been copyedited and formatted. The final version may differ from this version.

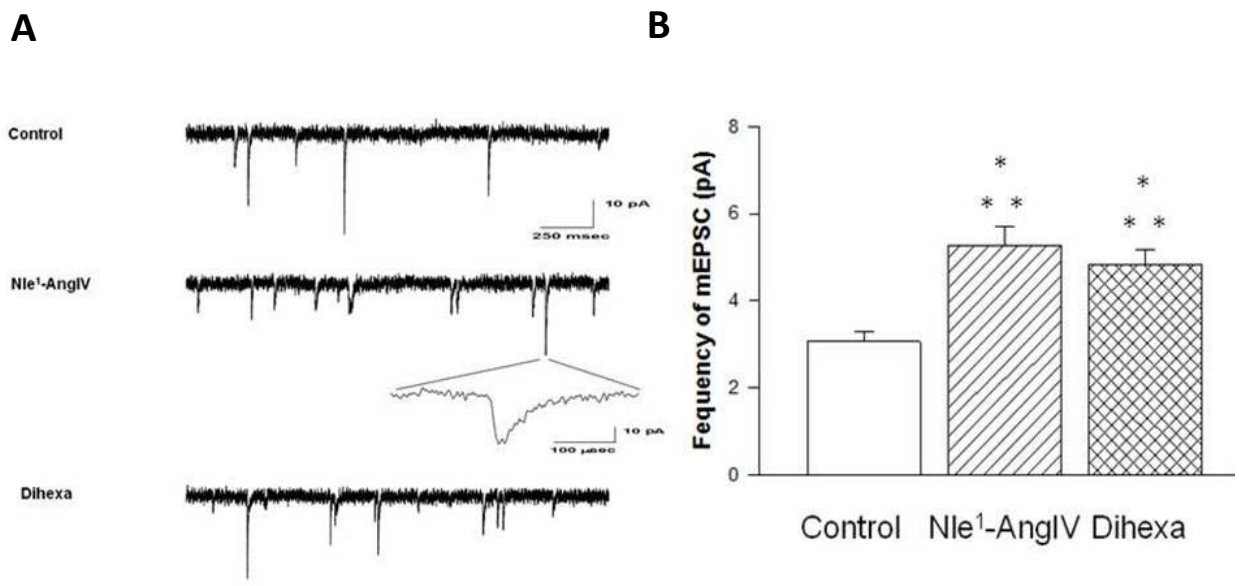


**Figure 8**